ABO Blood Sugar Antigen-Decorated Gold Nanoparticles as Nanotools for Biomedical Applications

Elena Di Marzo[1], Ruth Mateu Ferrando[1,2], Laura Polito[3], Laura Ragona[4], Katiuscia Pagano[4], Giuseppe D'Orazio[1], Luigi Lay[1]

Supporting Information

1. Synthesis of GAuNPs

1.1 Description of the microfluidic reactor

The flow within the microfluidic reactor was generated by a programmable peristaltic pump (LabCraft). The initial solution containing water/ethanol, glycan derivatives and $HAuCl_4$ was degassed before flowing in the tubes. The reaction zone was constituted by a FEP tube (Idex Health & Science LLC; 0.762 mm ID, 5 m length) coiled around a water-cooled UV lamp (125W, 100V, Helios Italquartz S.r.l). The circuit was closed, and the mixture was let flow in the tubes for 2 hours (Figure S1). The obtained GAuNPs were collected in a conical tube, purified and stored as 5 mL colloidal solution at 4 °C. The microreactor was fluxed with *aqua regia* ($HCl:HNO_3$ = 3:1) to remove possible residues of gold from the walls of the tubes at the end of each the reaction.

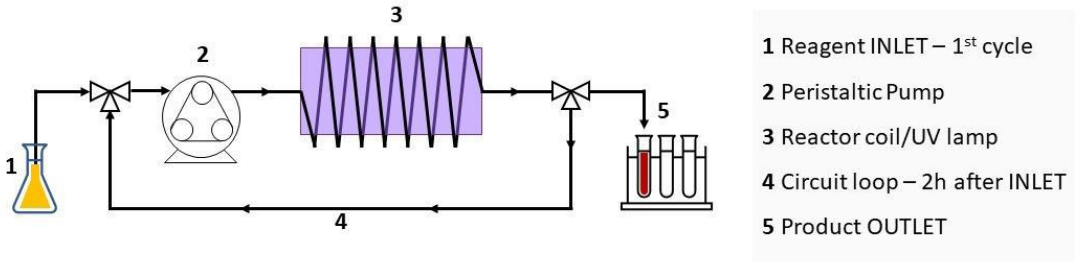

Figure S1. Scheme of the microfluidic reactor developed to produce GAuNPs.

Ligands	Concentration (mM)
4	14
5	3.3
6	3.4
5 + 6	1.8 +1.8

Table S1 – Concentration of sugar antigen derivatives **4**, **5** and **6** used for the synthesis of ABO-GAuNPs **1-4**.

2. NMR analyses on GAuNPs

2.1 Estimation of antigen groups on ABO-GAuNP

NMR spectra were recorded at 25°C on a Bruker AvanceIII spectrometer operating at 500 MHz and processed with the software Topspin 4.3.0. The ABO-GAuNPs samples were lyophilized and re-dispersed in 600 µL of D_2O for NMR spectroscopy. In Figure S2A we report the comparison of selected regions of the ^{1}H-NMR spectra recorded on free ligands and ABO Antigen-UAuNPs. The strong broadening of the proton resonances in the direct surroundings of thiol groups of the ligand (Hβ at ~ 2.4 ppm) observed in the spectra recorded for ABO-GAuNPs samples confirms the binding of ligands to the gold nanoparticles.

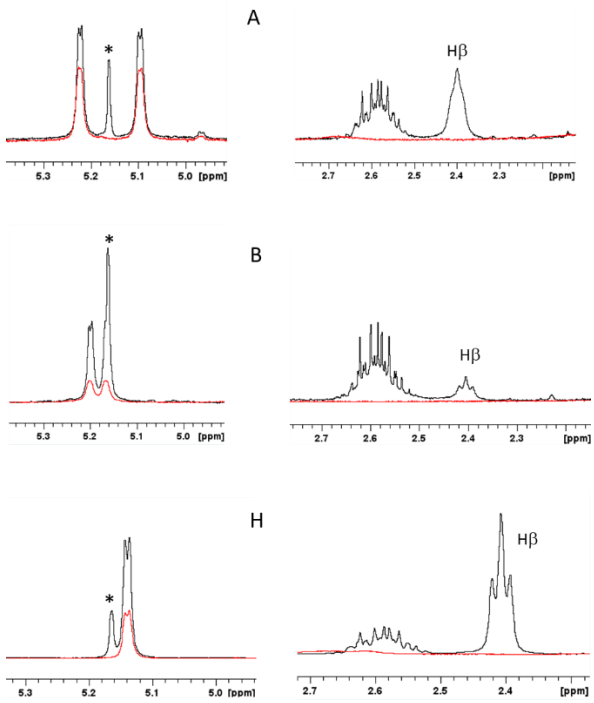

Figure S2. Overlap of ^{1}H-NMR spectra recorded for free ligands (black) and ABO-GAuNPs samples (red). Anomeric and Hβ regions are displayed for antigen A (upper panel), B (central panel) and H (lower panel). * marks impurities observed in free ligand samples.

In order to quantify ligand loaded on GAuNPs, samples were analyzed by NMR using the ERETIC 2 (Electronic REference To access *In vivo* Concentrations) methodology. ERETIC 2 is an experimental quantitative NMR technique based on PULCON (pulse length-based concentration determination) [1], an internal standard method which correlates absolute intensities of two different spectra. A sucrose sample of known concentration (29.2 mM), under "quantitative" condition was employed as reference: probe was exactly tuned and matched, 90° pulse calibrated, D1 relaxation delay time 10 s (>5*T1), acquisition time 4 s (>T2), SW=29 ppm, NS=64. Anomeric signals, free from overlap, were selected for integration. The molarity of antigen coated on UAuNPs, determined by ERETIC NMR, is reported in Table S1. ERETIC NMR analysis indicated an equivalent uploading of A and B antigens on NP coating when an equimolar mixture of the two antigens was employed.

GauNP sample	Sugar ligand concentration (mM)
GAuNP1	5.9
GAuNP2	2.1
GAuNP3	1.7
GAuNP4	0.75 + 0.75

Table S1 Estimation of Antigen concentration in 600 µL sample of ABO-GAuNPs.

2.2 Hydrodynamic radius determination (NMR-DOSY experiments)

^{1}H-DOSY experiments (diffusion-ordered spectroscopy) were performed on functionalized NPs purified sample. Matrices of 16384 (t2) by 80 points (t1) were collected. The z-axis gradient strength was varied linearly from 2 to 98% of its maximum value (53 G cm^{-1}), the gradient pulse duration was 4.4 ms, and the time period between the two gradient pulses was optimized to 200 ms. Self-diffusion coefficients (D) were derived by fitting the NMR data to Stejskal and Tanner equation [2]. Averaged D values derived from DOSY spectra (Figure S3) are reported in Table S2.

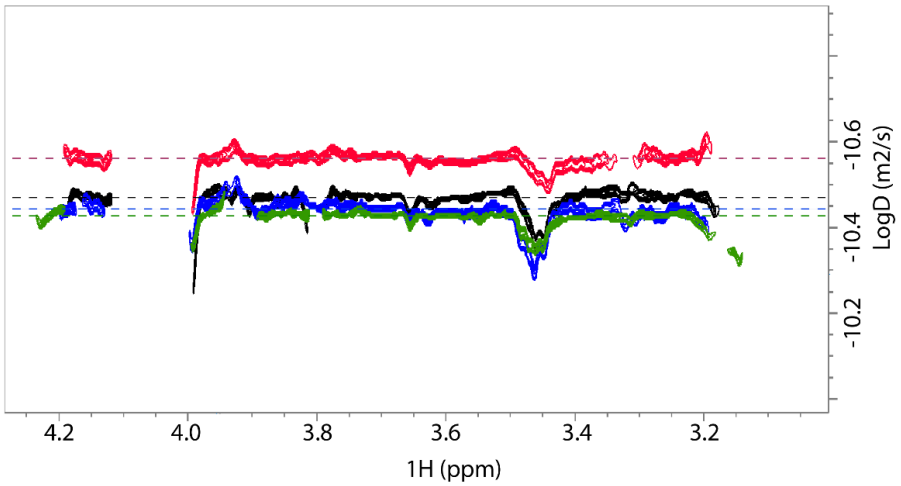

Figure S3. Overlay of ^{1}H DOSY NMR spectra of GAuNP3 (black), GAuNP2 (blue), GAuNP4 (red), and GAuNP1 (green) dissolved in D_2O at 25°C. Dashed lines correspond to averaged D values reported in Table S2.

NP sample	D x 10^{-11} (m2/s)	R hydro (nm)
GAuNP1	3.7 ± 0.1	4.9 ± 0.1
GAuNP2	3.4 ± 0.1	5.4 ± 0.1
GAuNP3	3.6 ± 0.1	5.1 ± 0.1
GAuNP4	2.7 ± 0.1	6.6 ± 0.1

Table S2. Averaged D values derived from DOSY spectra and hydrodynamic radii derived from equation [2]

Assuming a spherical geometry for **GAuNPs**, the Stokes-Einstein equation [1] allows to derive NP hydrodynamic radii, using an internal standard (dioxane). The Stokes–Einstein equation [1] correlates the diffusion coefficient of a molecule with its hydrodynamic radii [3–5]:

$$r_H = \frac{k_B T}{6\pi\eta D} \qquad [1]$$

where r_H is the hydrodynamic radius, k_B the Boltzmann constant, T the temperature in K, η the dynamic viscosity of D2O at 25 °C, and D the measured translational diffusion coefficient.

Using the diffusion measured for dioxane molecule, added to the sample as internal standard, hydrodynamic radii reported in Table S2 were derived using equation [2] [6,7]:

$$r_H^{NP} = r_H^{diox} \times \frac{D_{diox}}{D_{NP}} \qquad [2]$$

considering r_H^{diox}=0.212 nm.

Inverse Laplace Transform (ILT) reconstruction method was employed within the Bruker Dynamics Center software suite, version 2.6.1, to derive NP's hydrodynamic radius distributions from NMR diffusion measurements.

3. TEM Characterization of GAuNPs

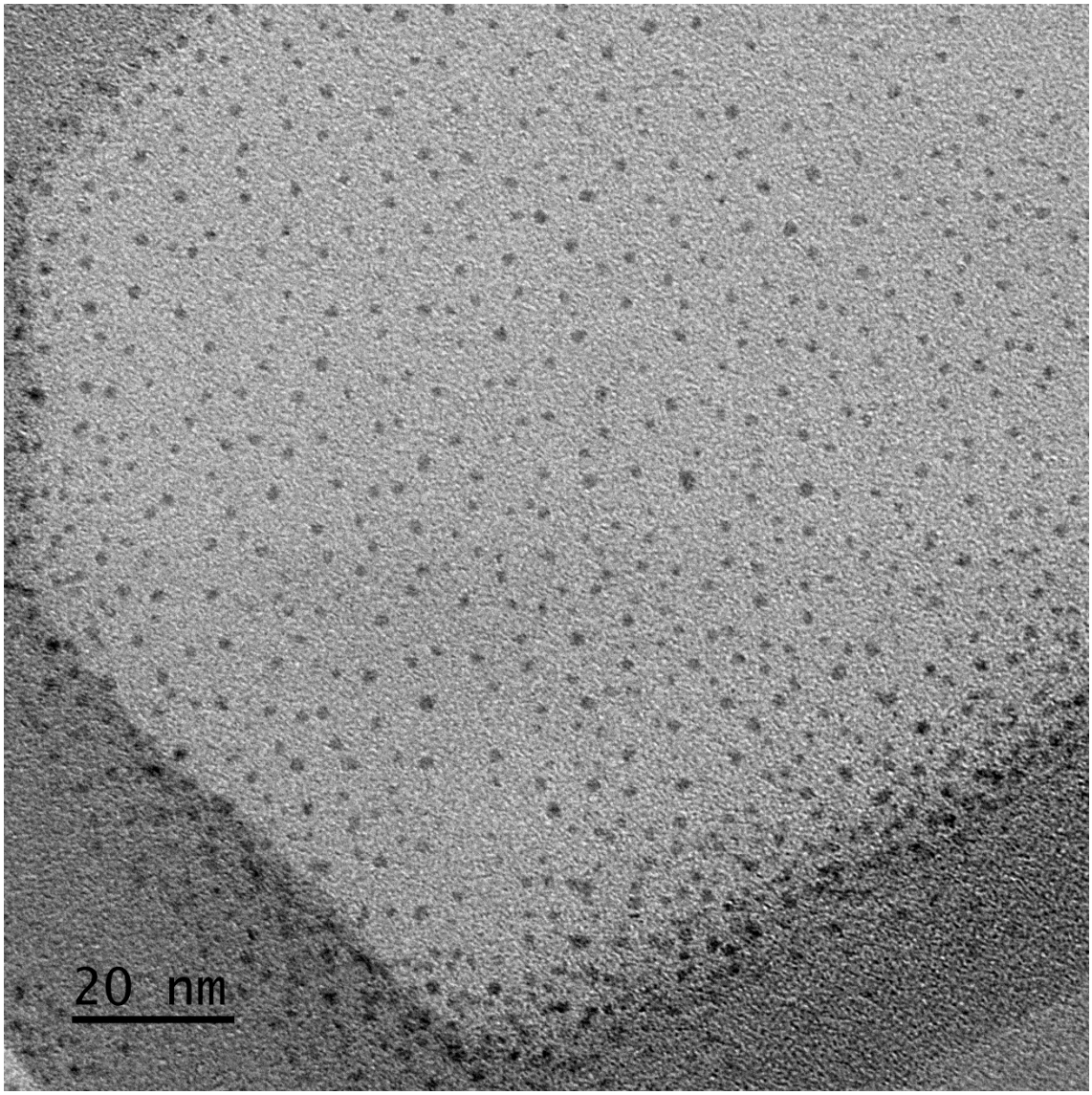

Figure S5. TEM micrograph of GAuNP1.

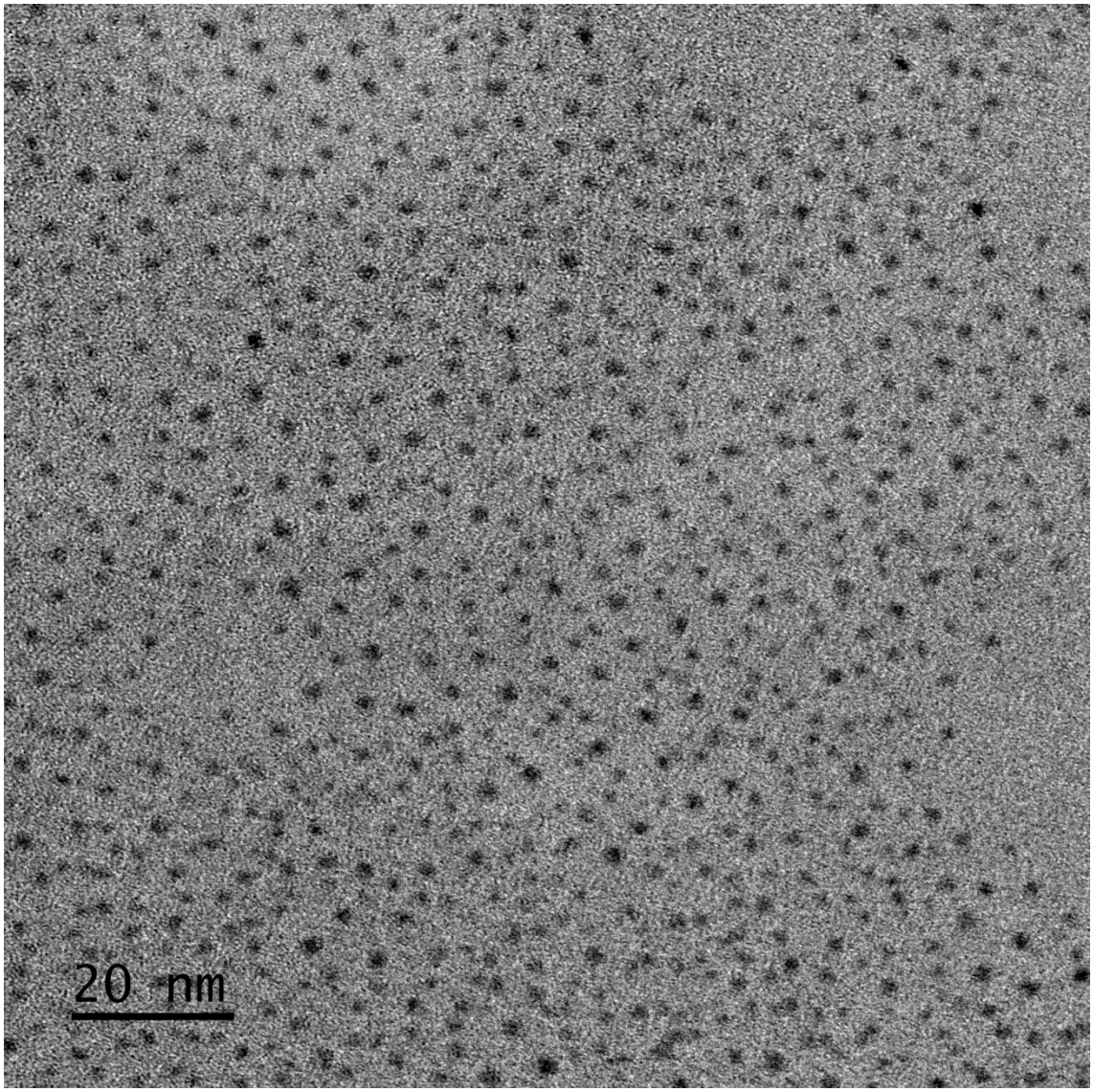

Figure S5. TEM micrograph of GAuNP2.

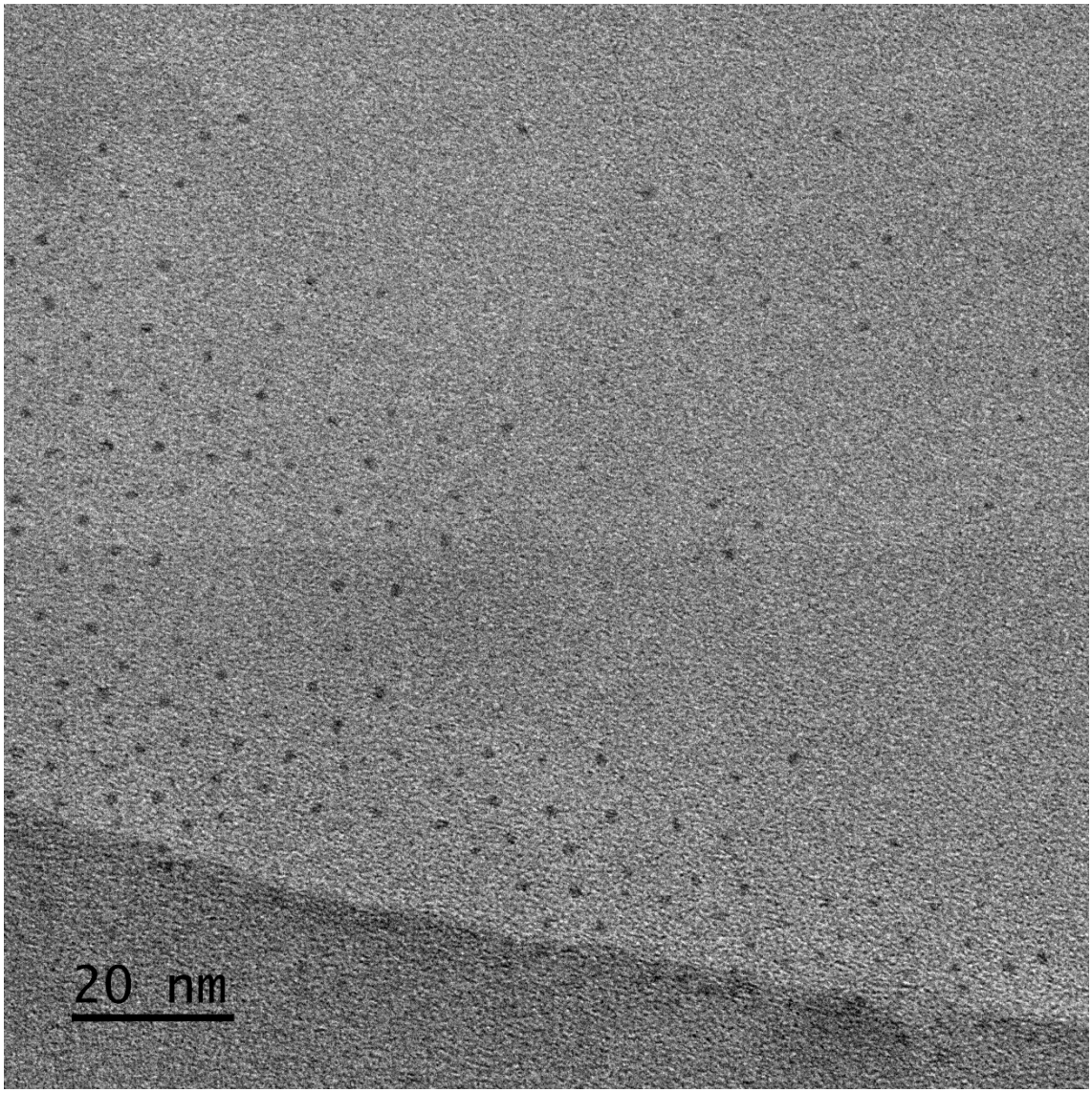

Figure S5. TEM micrograph of GAuNP3.

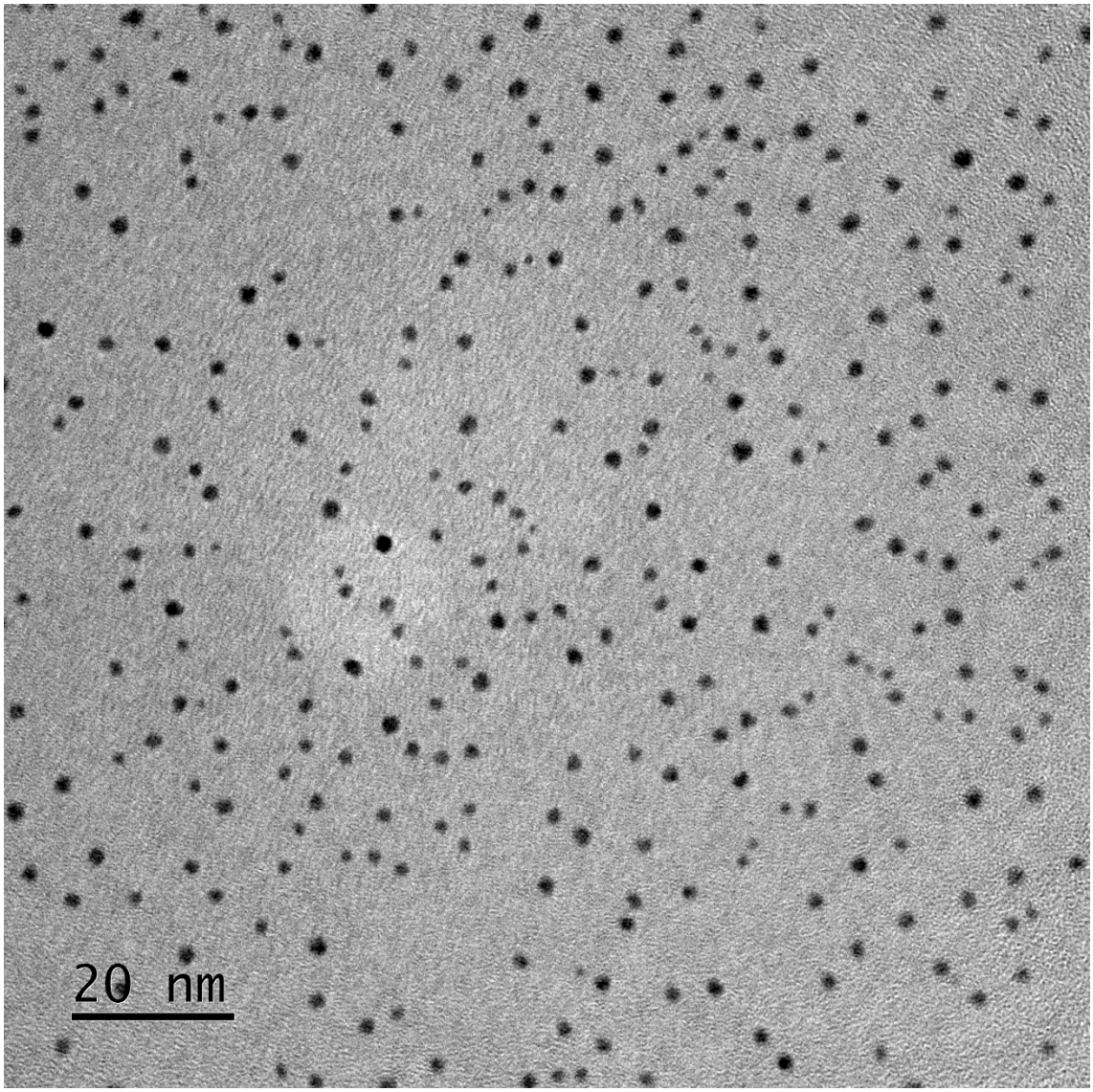

Figure S5. TEM micrograph of GAuNP4.

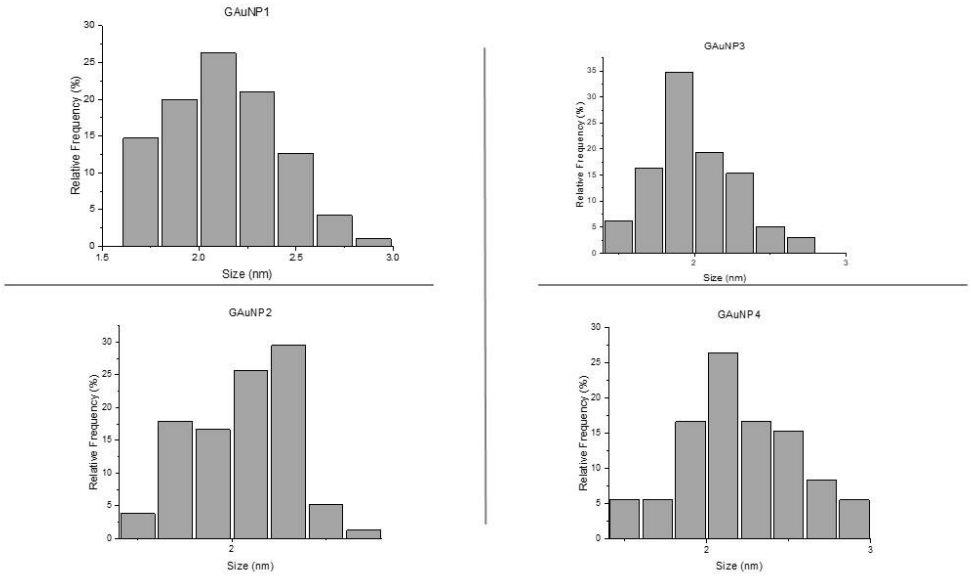

Figure S6. Size distribution (nm) GAuNPs 1-4. The median diameter for each sample is: **GAuNP1**: 2.1 nm; **GAuNP2**: 2.0 nm; **GAuNP3**: 2.0 nm; **GAuNP4**: 2.2 nm

4. ^{1}H and ^{13}C NMR spectrum of synthesized compounds

Compound 1

^{1}H-NMR (400 MHz, D_2O)

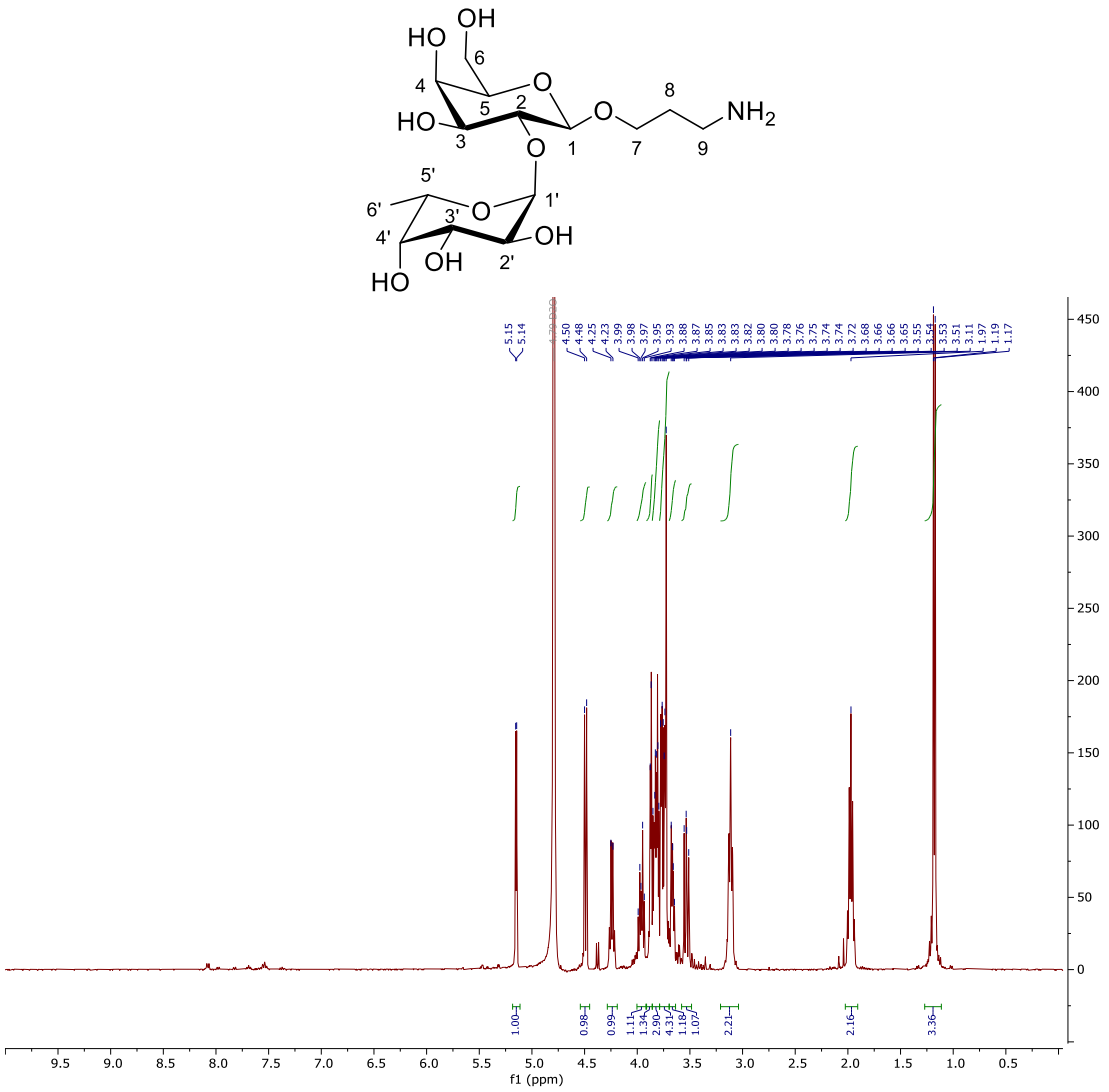

^{13}C-NMR (100 MHz, D_2O)

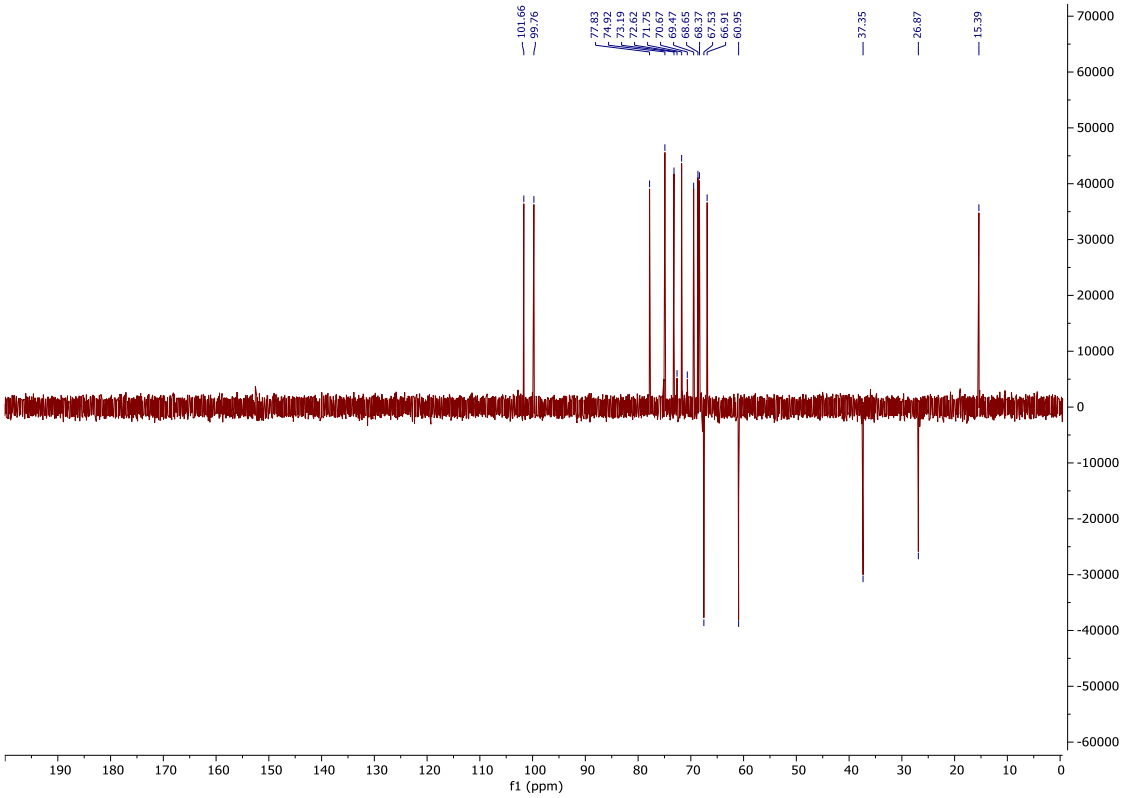

Compound 2

^{1}H-NMR (400 MHz, D_2O)

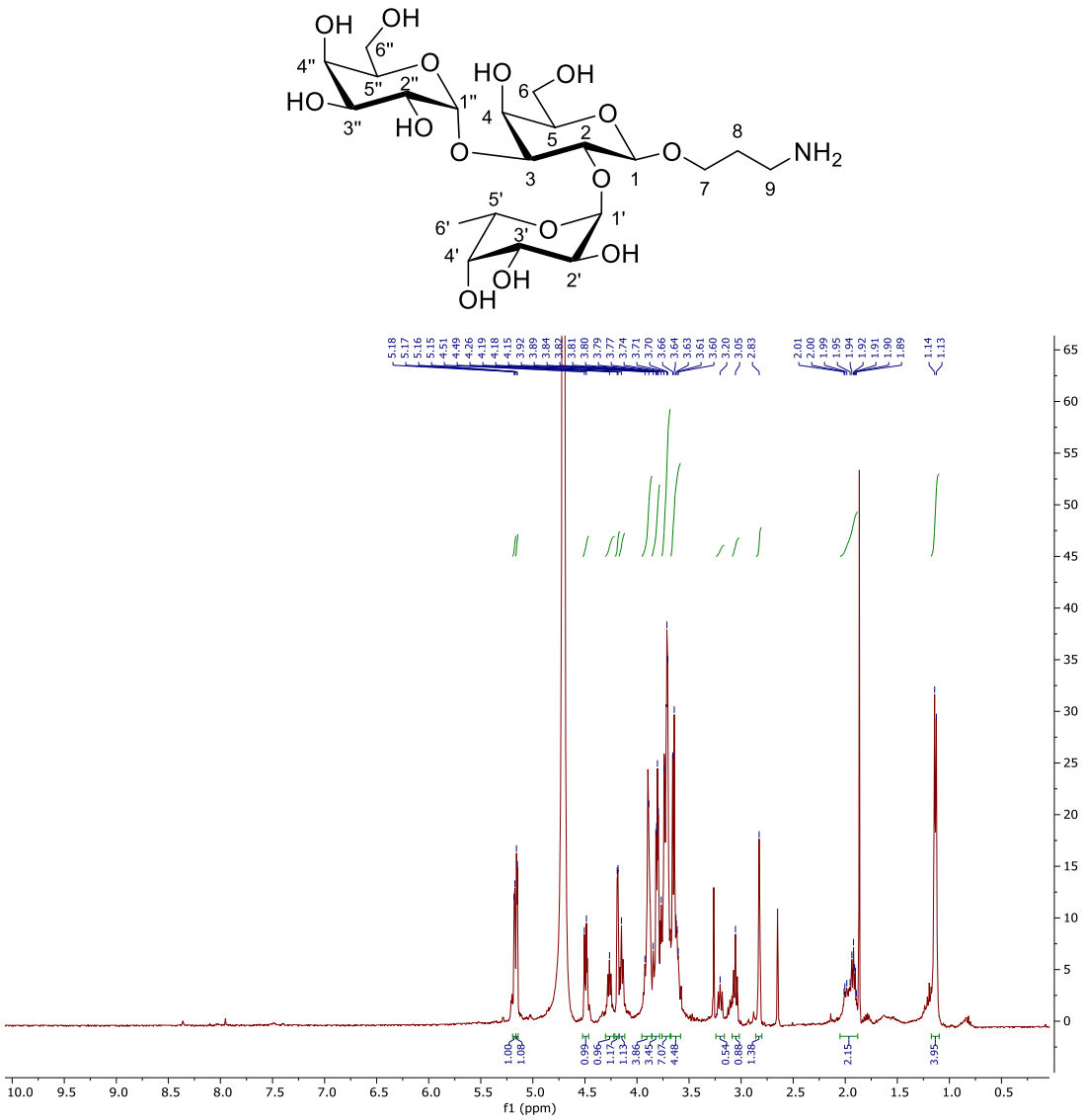

^{13}C-NMR (100 MHz, D_2O)

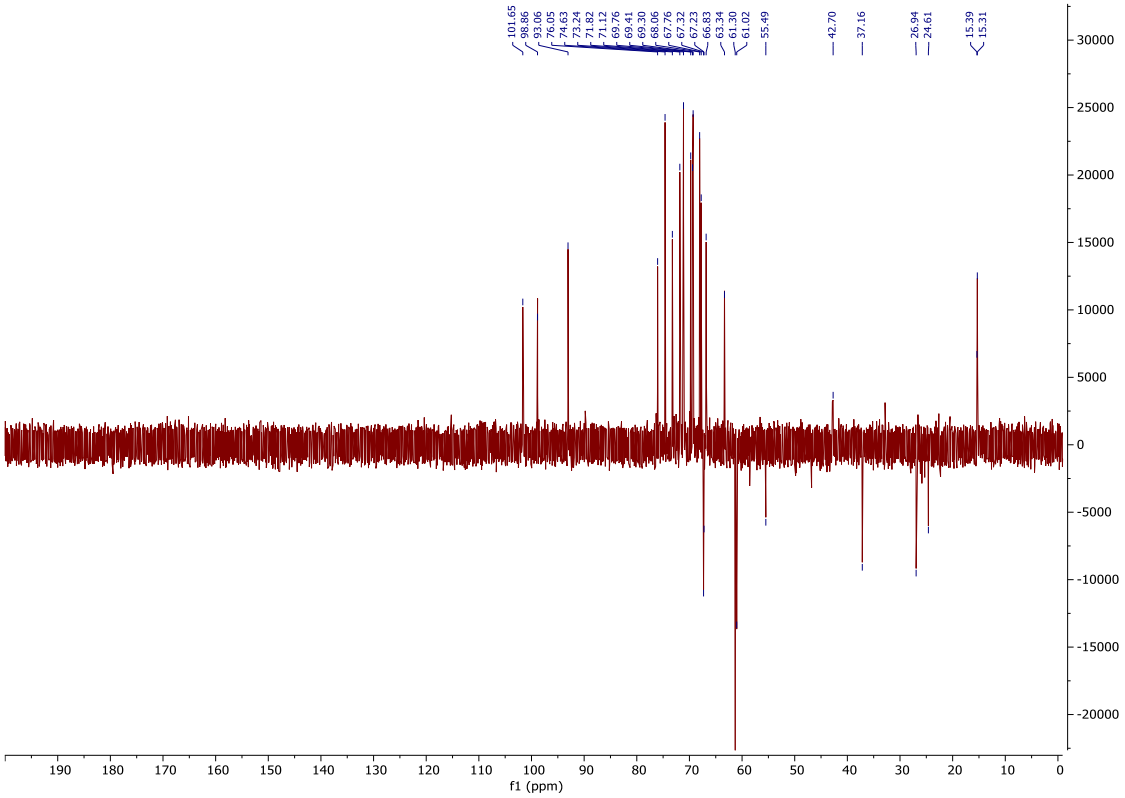

Compound 3

^{1}H-NMR (400 MHz, CD_3OD)

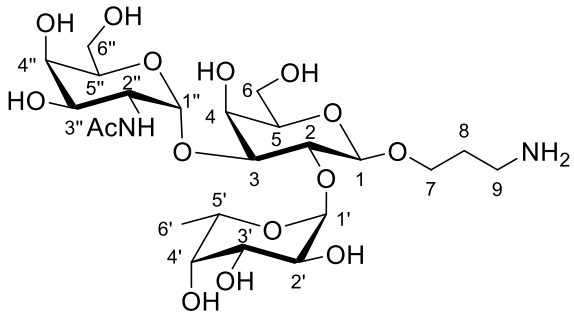

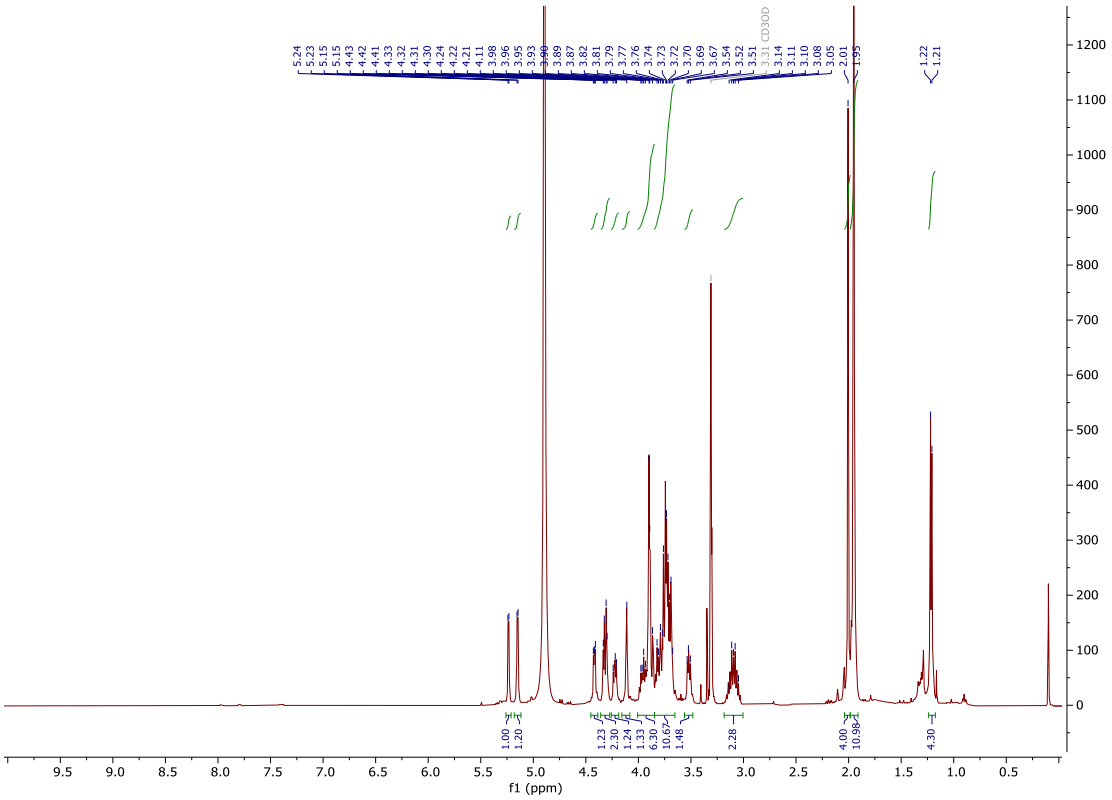

^{13}C-NMR (100 MHz, CD_3OD)

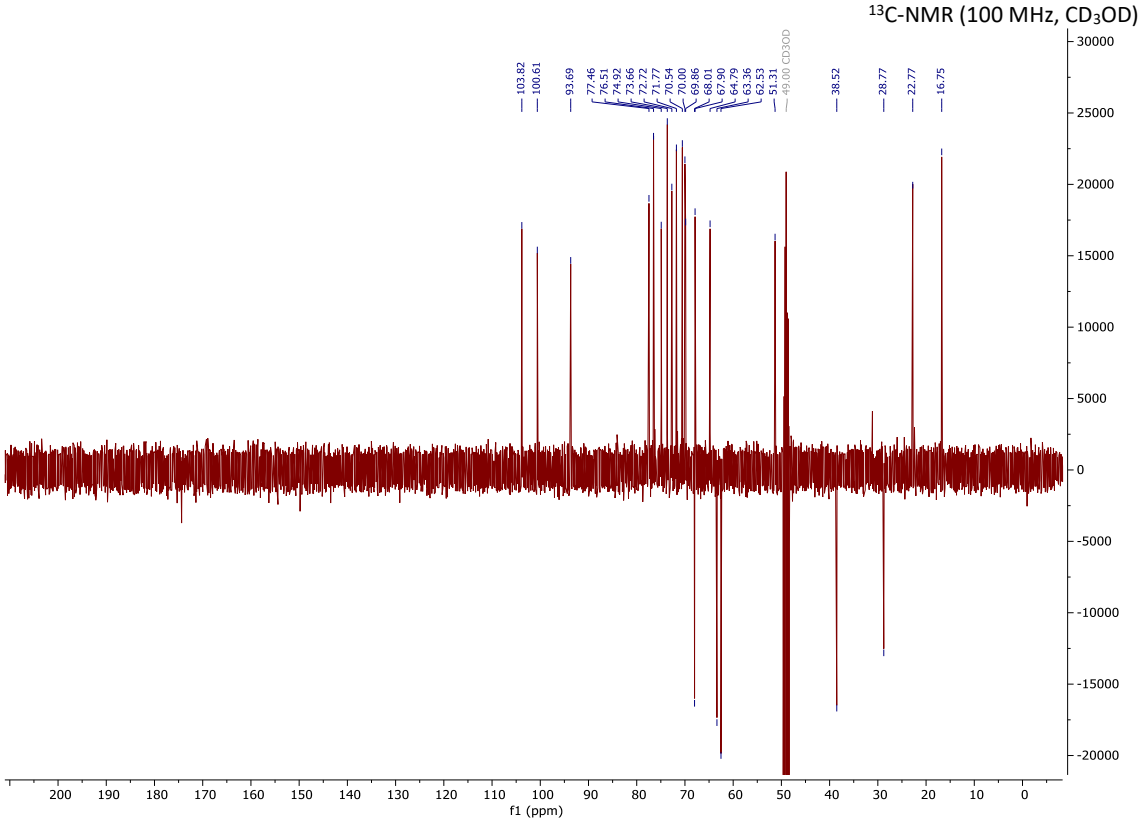

Compound 4

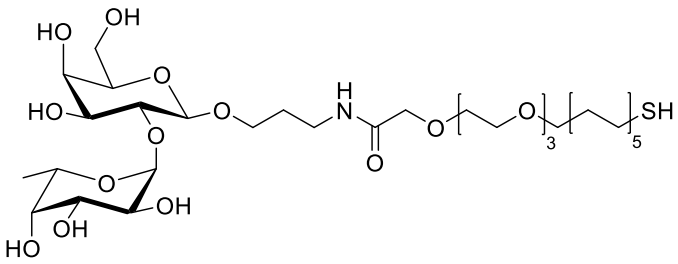

^{1}H-NMR (400 MHz, CD_3OD)

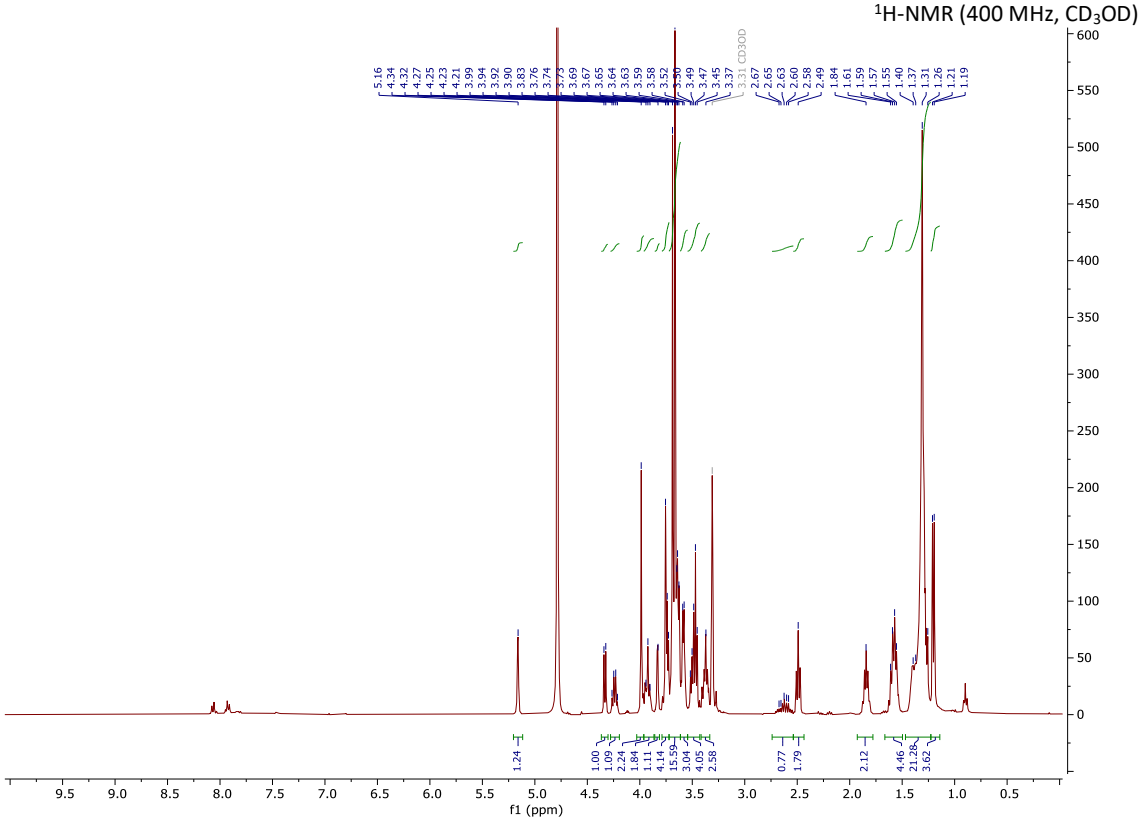

Compound 5

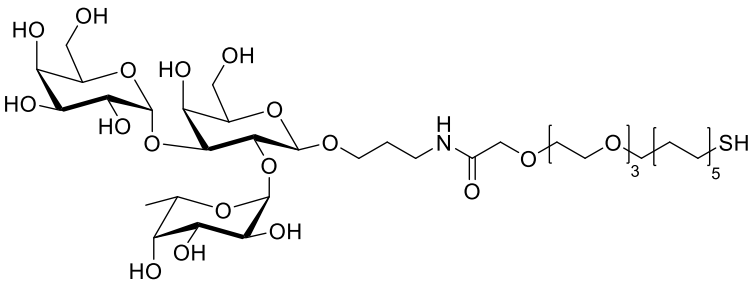

^{1}H-NMR (400 MHz, CD_3OD)

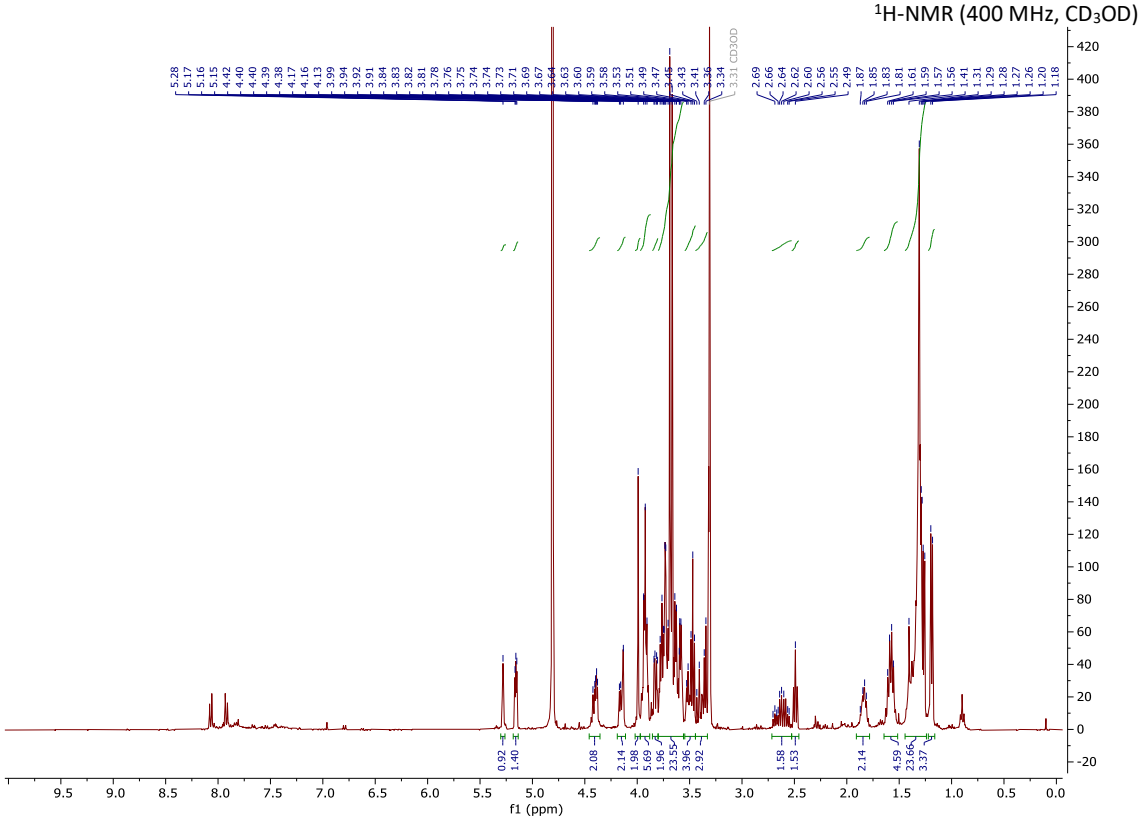

Compound 6

^{1}H-NMR (400 MHz, CD_3OD)

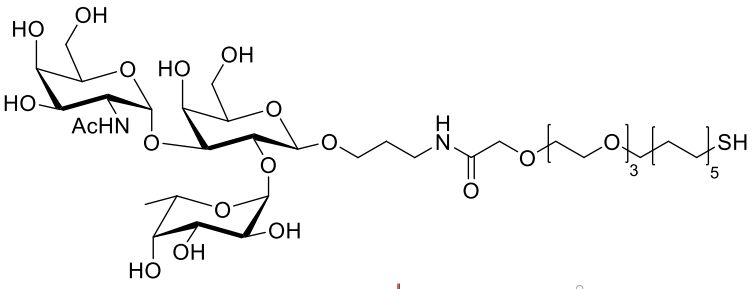

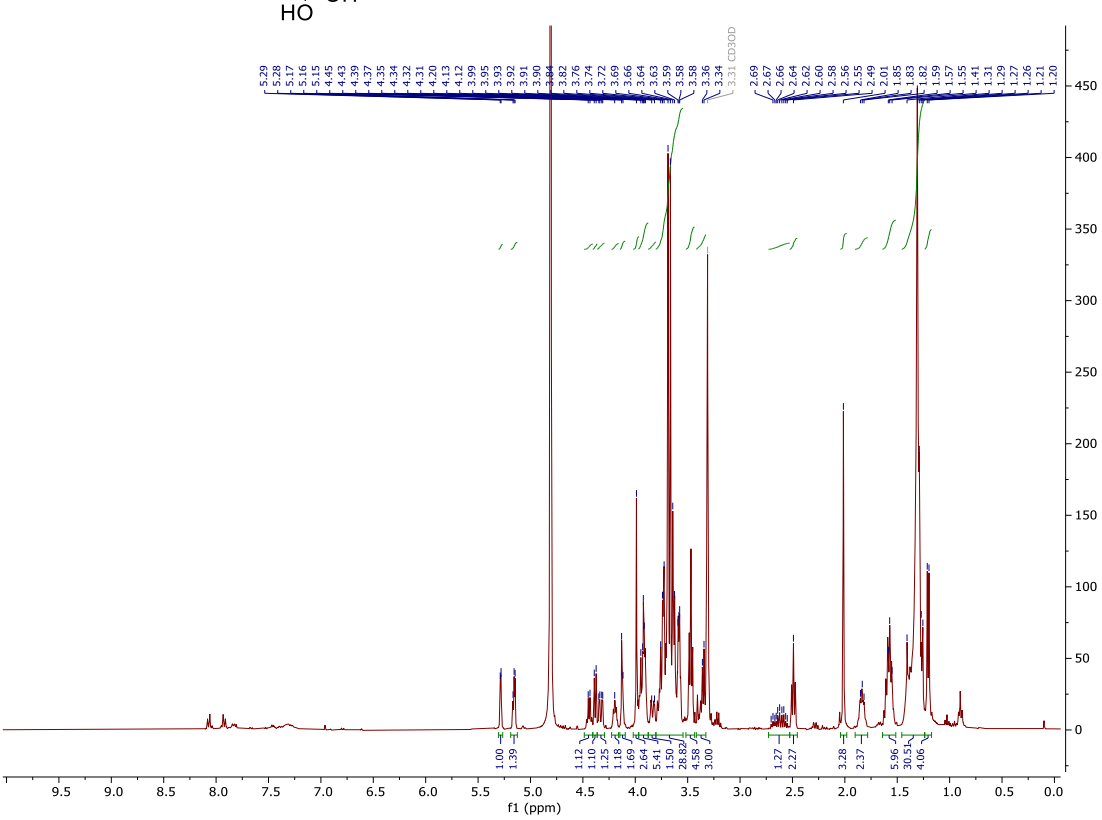

Compound 8

^{1}H-NMR (400 MHz, $CDCl_3$)

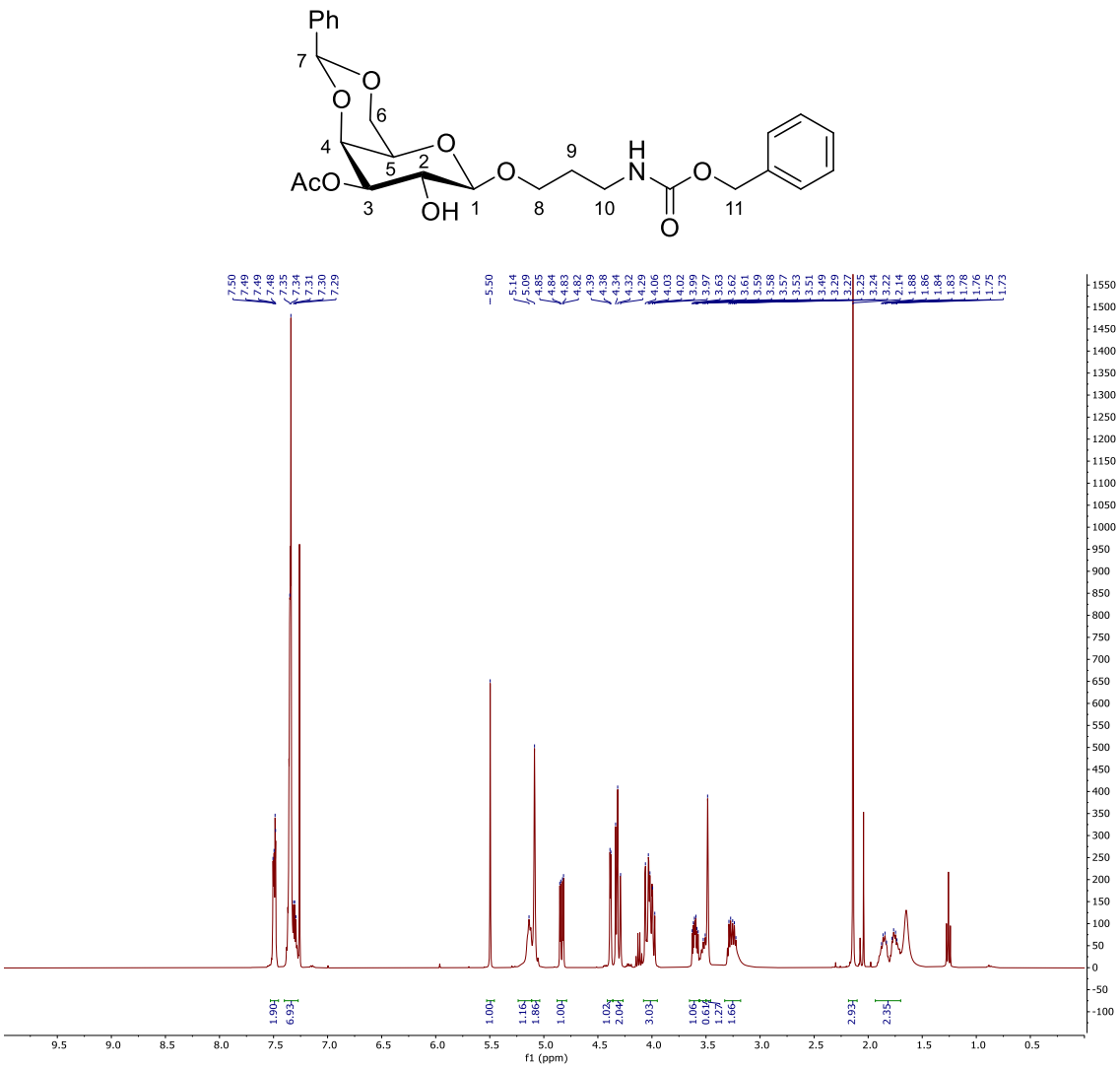

^{13}C-NMR (100 MHz, $CDCl_3$)

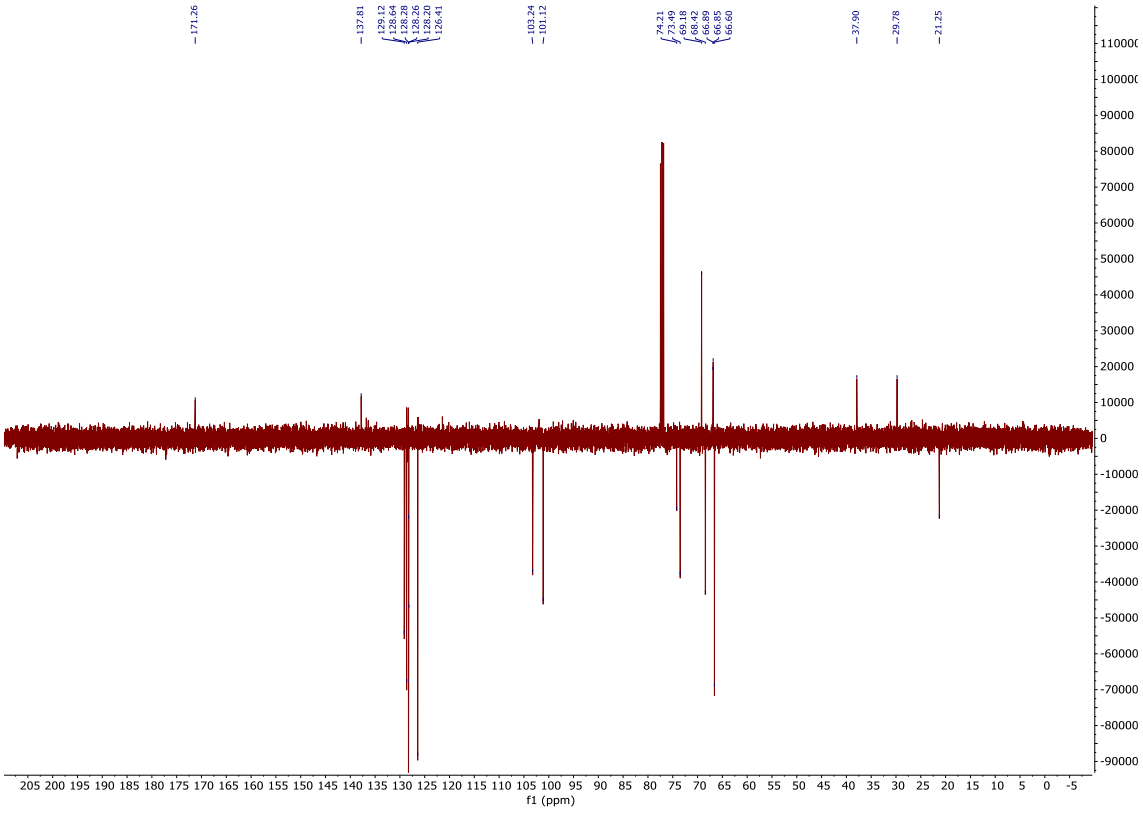

Compound 10

^{1}H-NMR (400 MHz, $CDCl_3$)

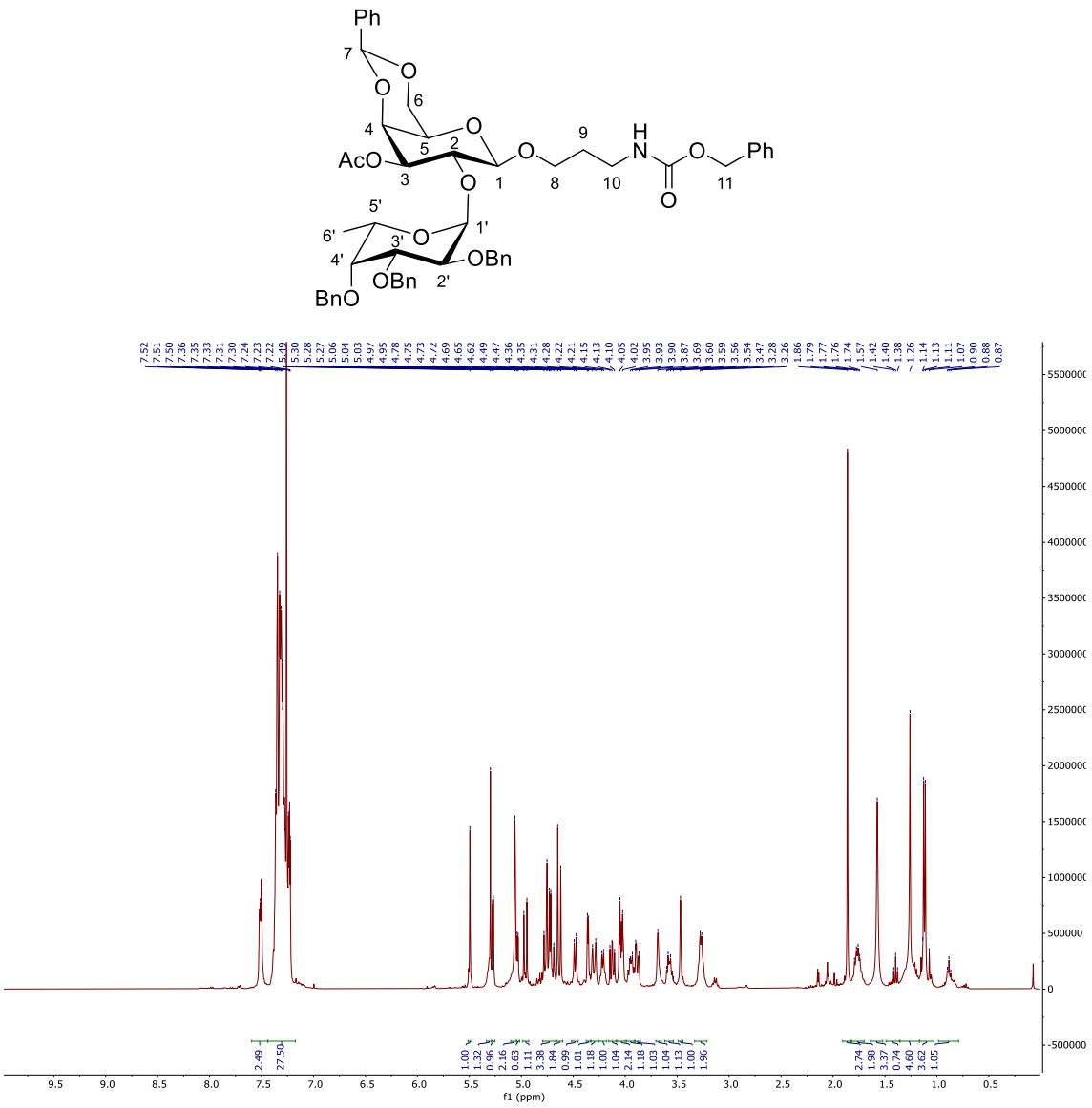

^{13}C-NMR (100 MHz, $CDCl_3$)

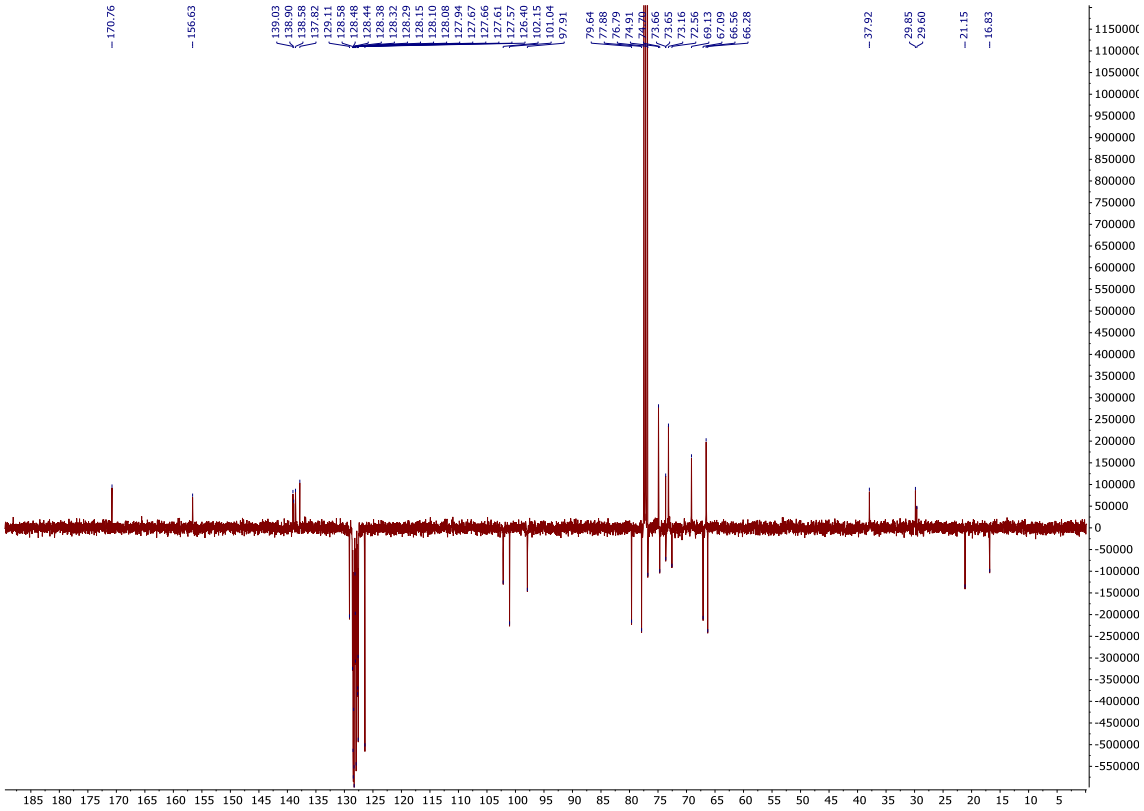

Compound 11

^{1}H-NMR (400 MHz, $CDCl_3$)

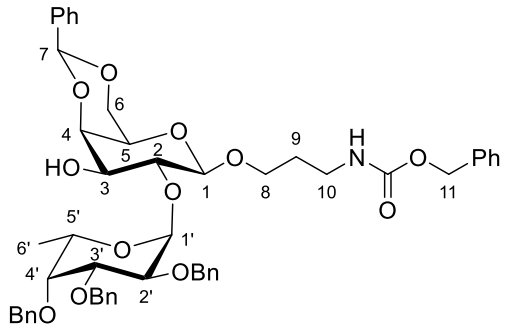

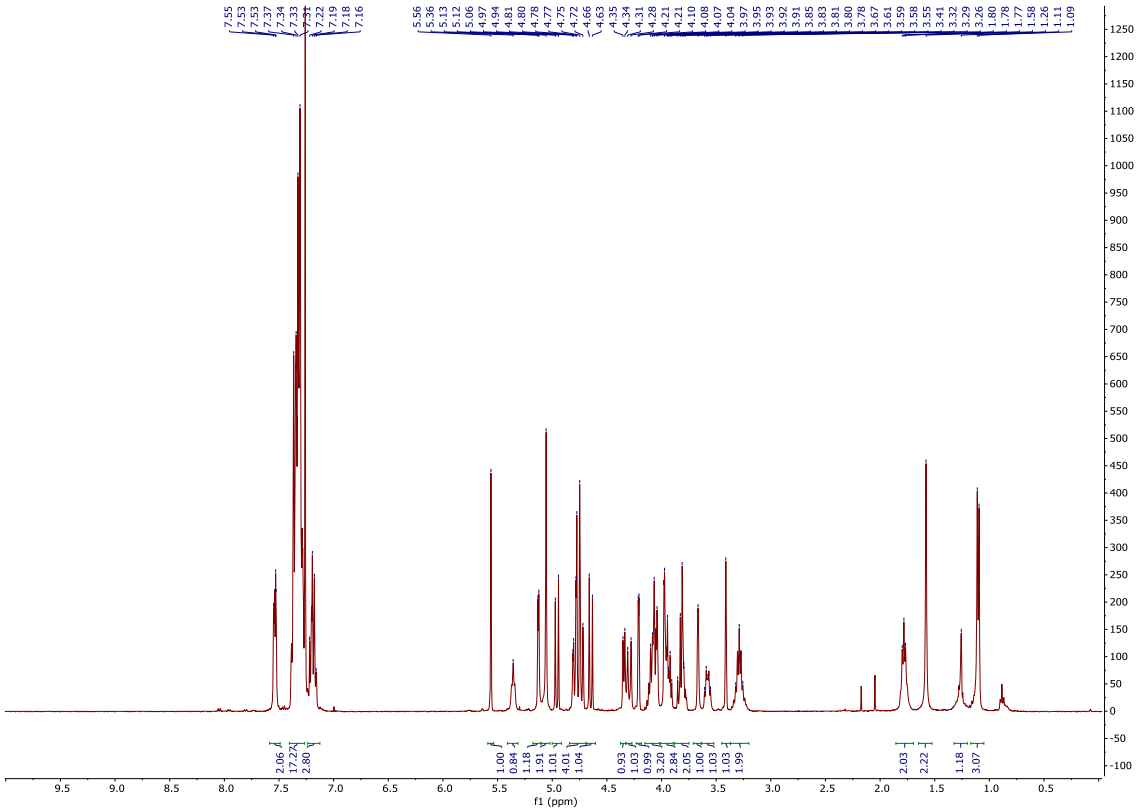

^{13}C-NMR (100 MHz, $CDCl_3$)

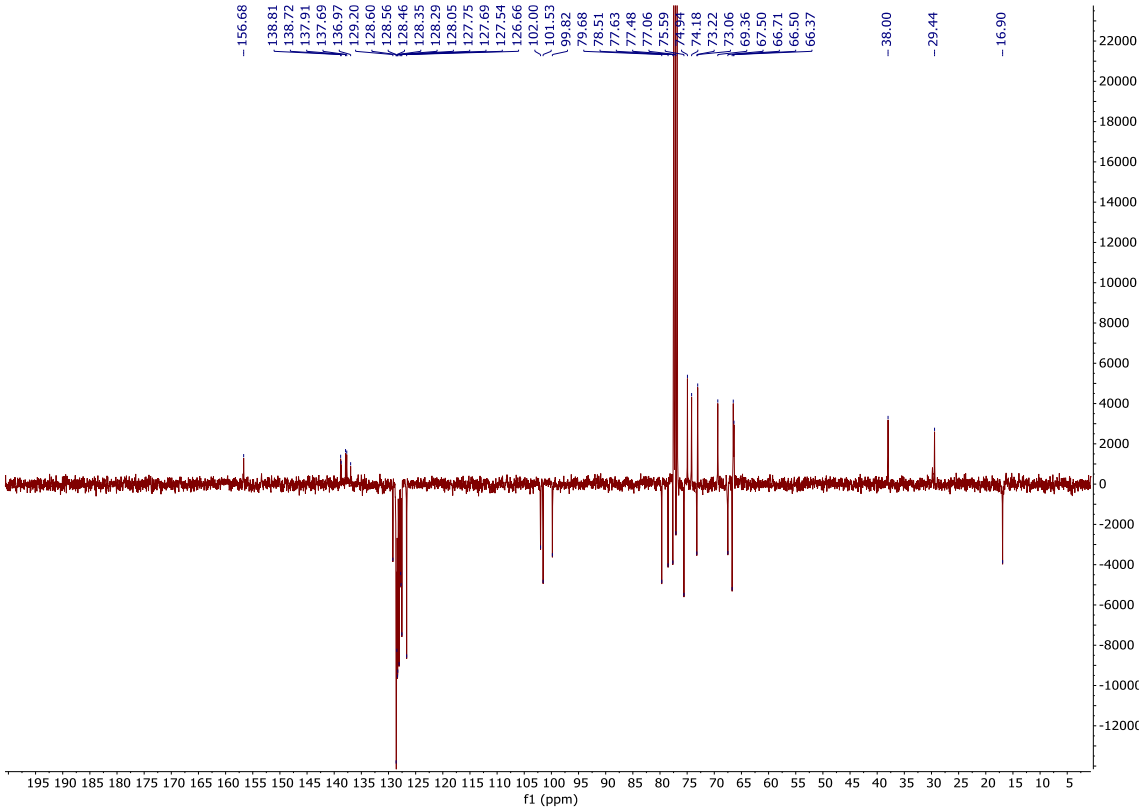

Compound 13

^{1}H-NMR (400 MHz, $CDCl_3$)

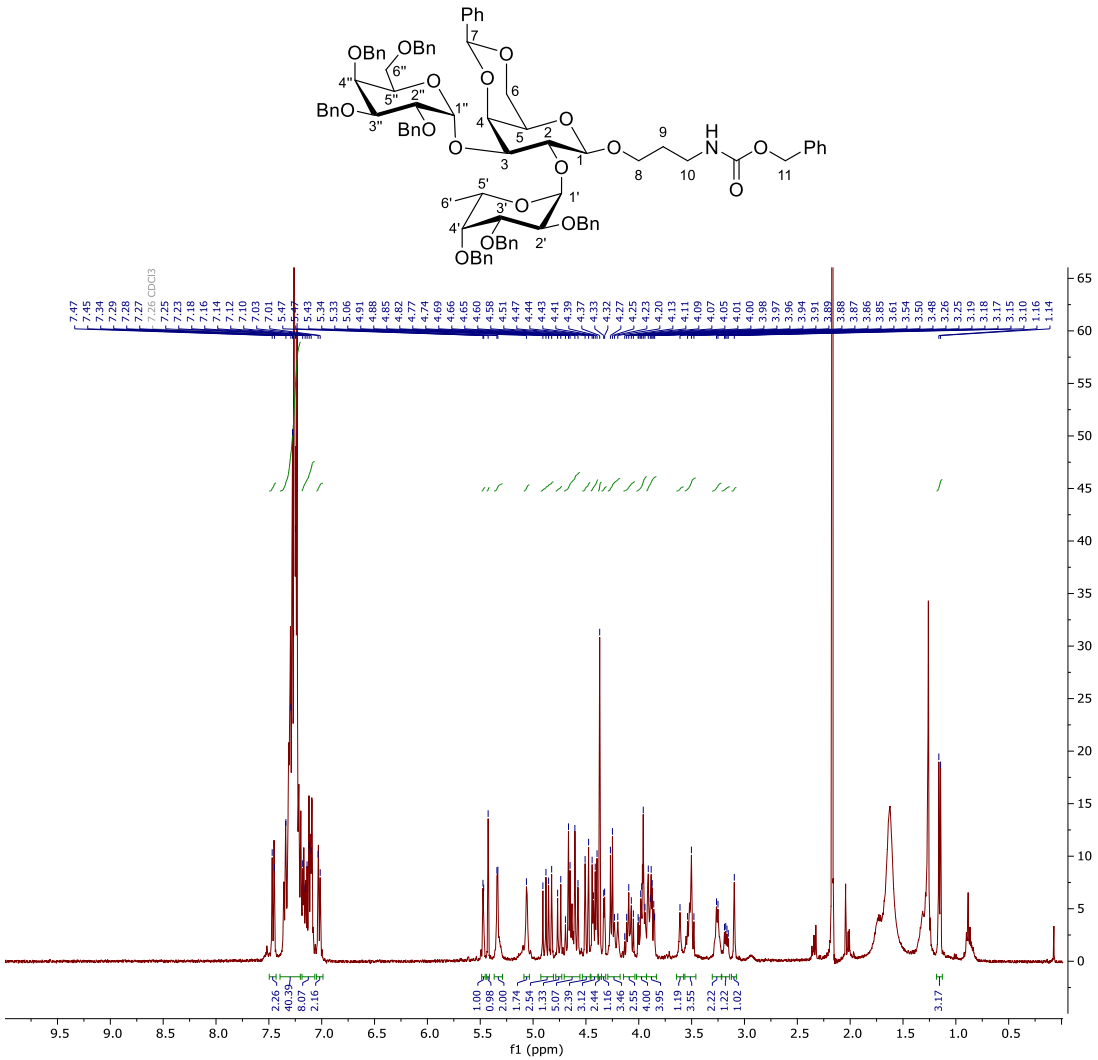

^{13}C-NMR (100 MHz, $CDCl_3$)

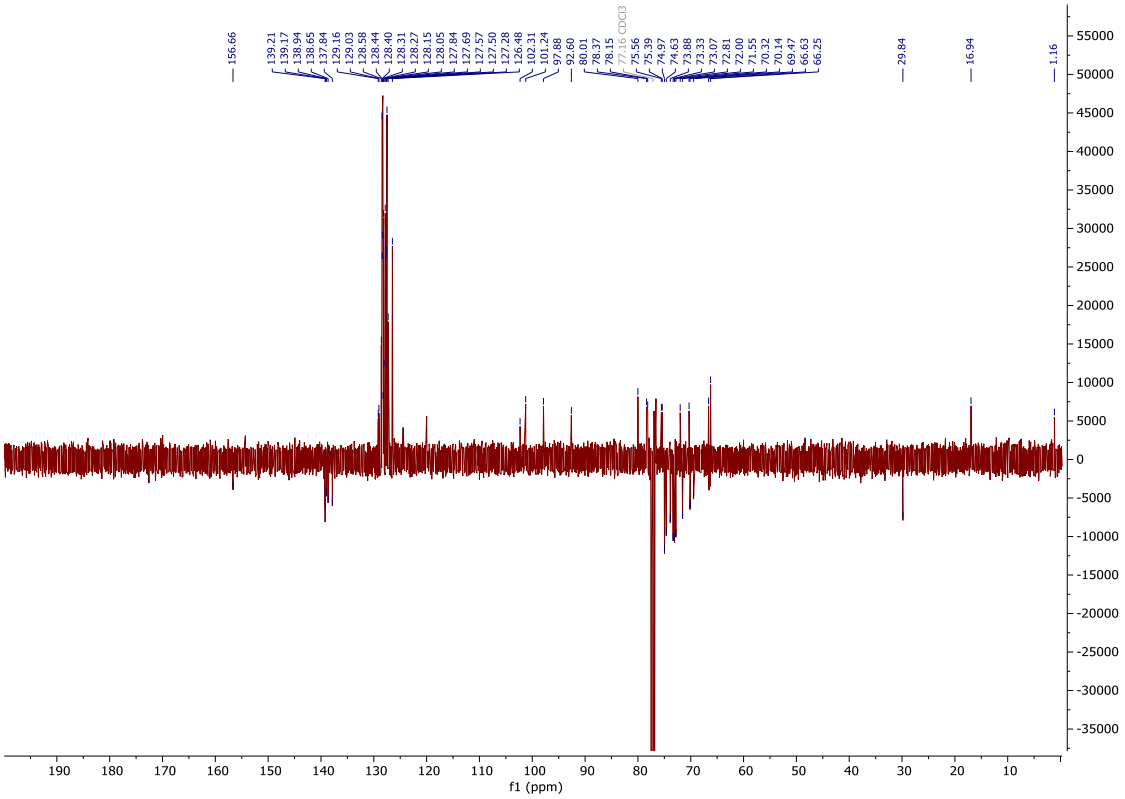

Compound 15

^{1}H-NMR (400 MHz, $CDCl_3$)

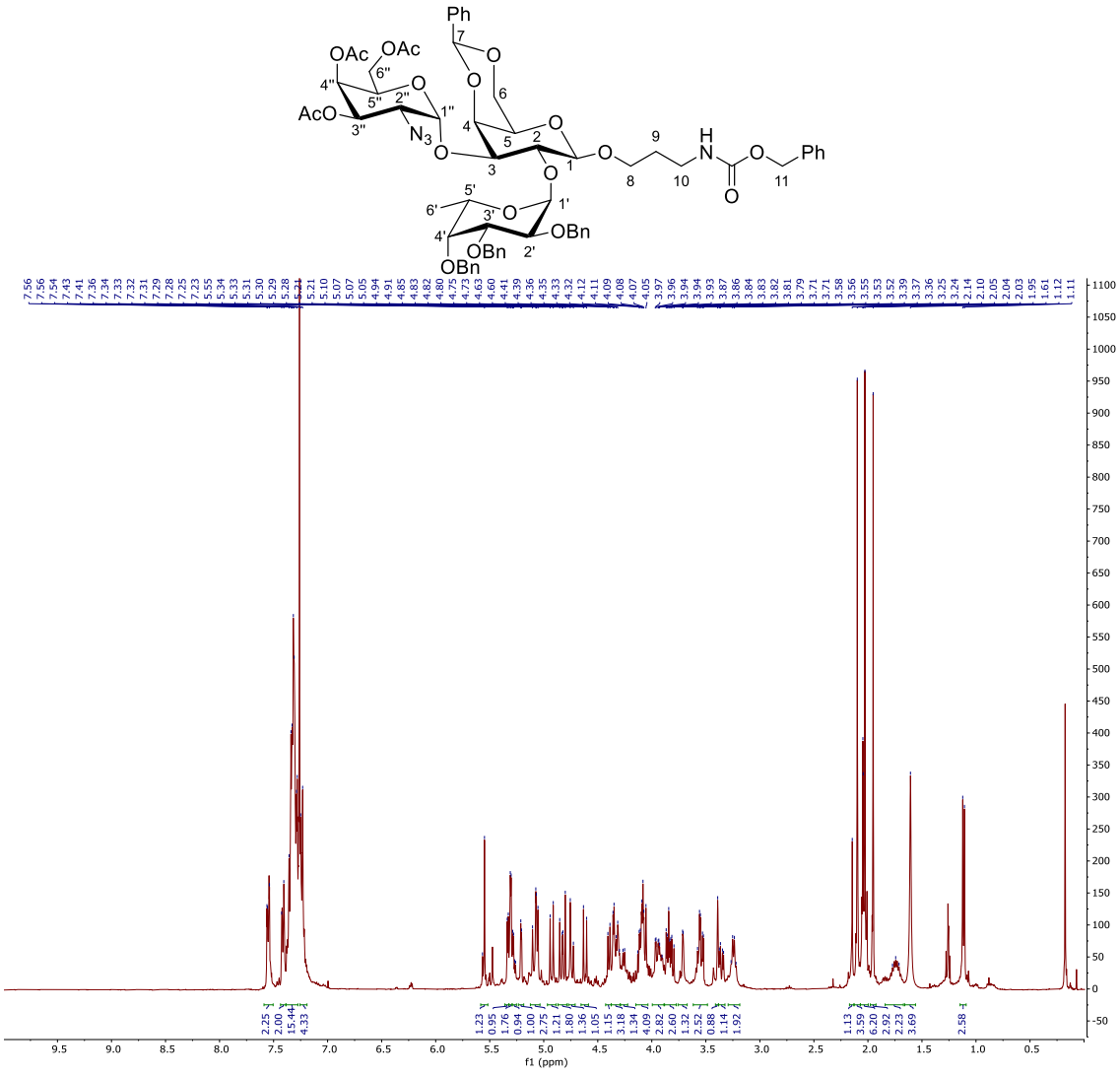

^{13}C-NMR (100 MHz, $CDCl_3$)

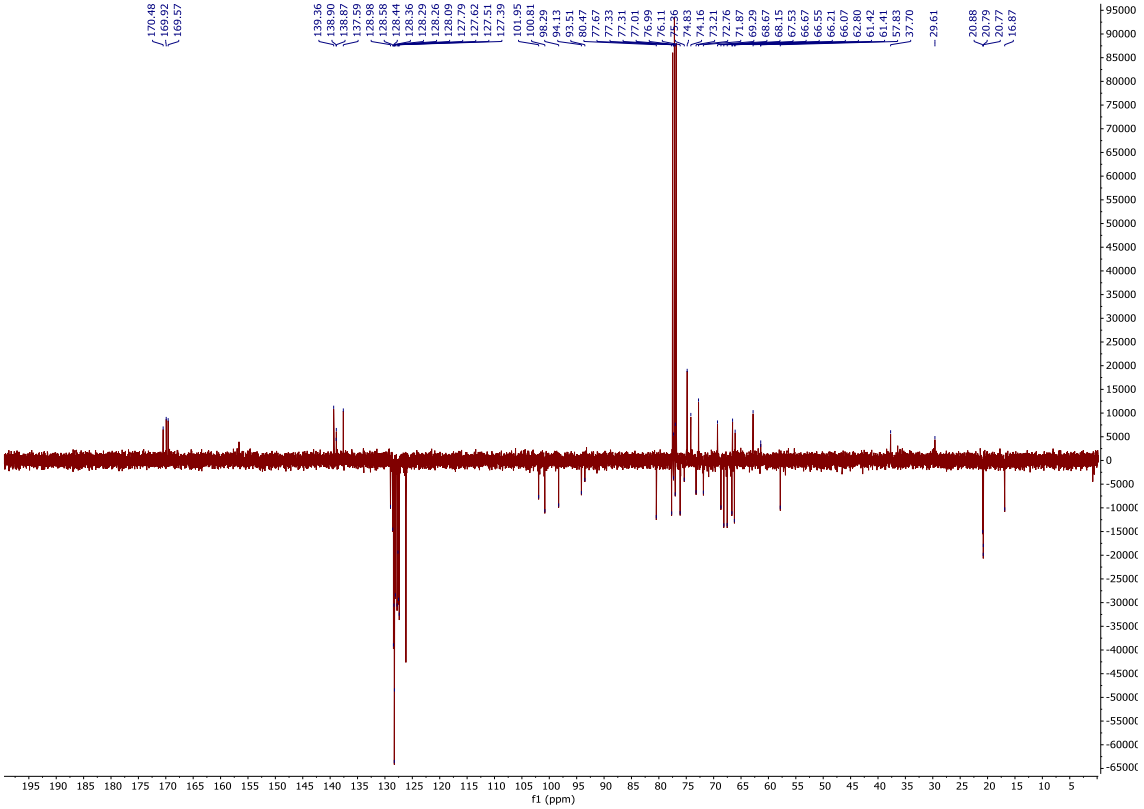

Compound 16

^{1}H-NMR (400 MHz, CD_3OD)

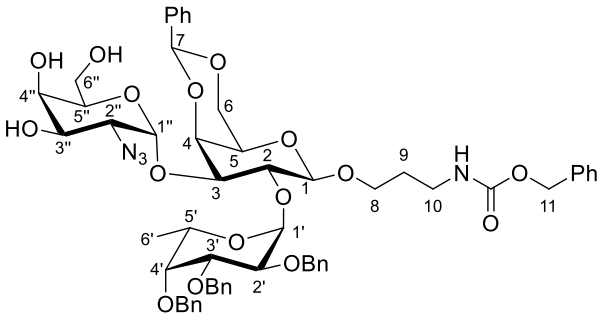

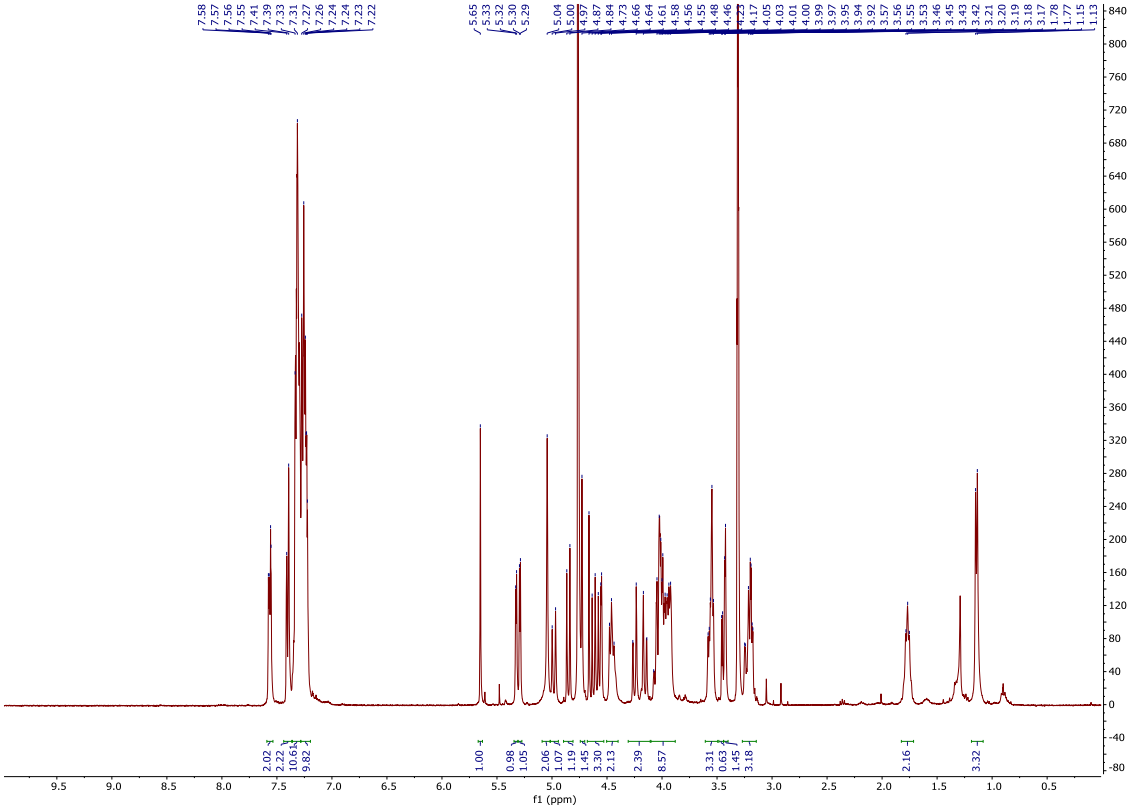

^{13}C-NMR (100 MHz, CD_3OD)

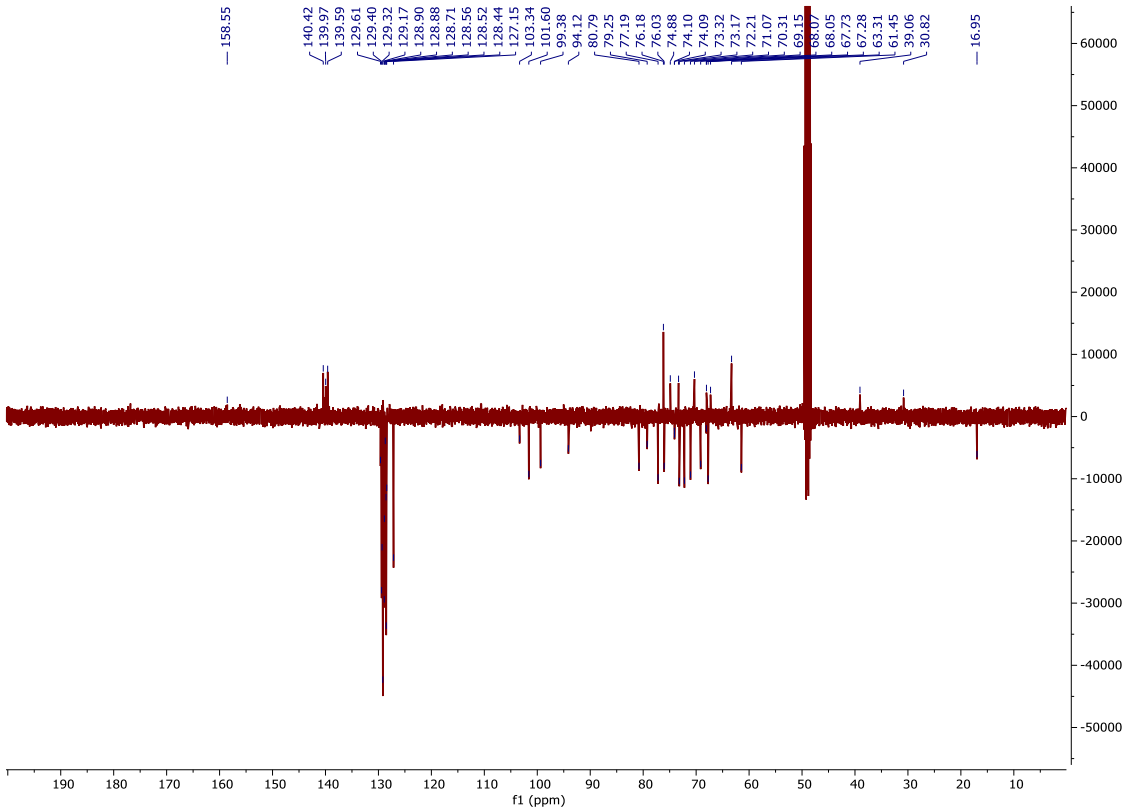

Compound 18

^{1}H-NMR (400 MHz, CD_3OD)

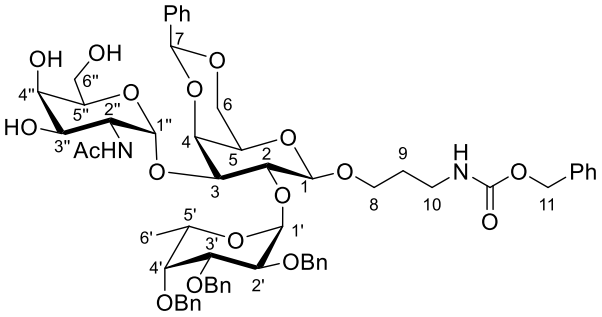

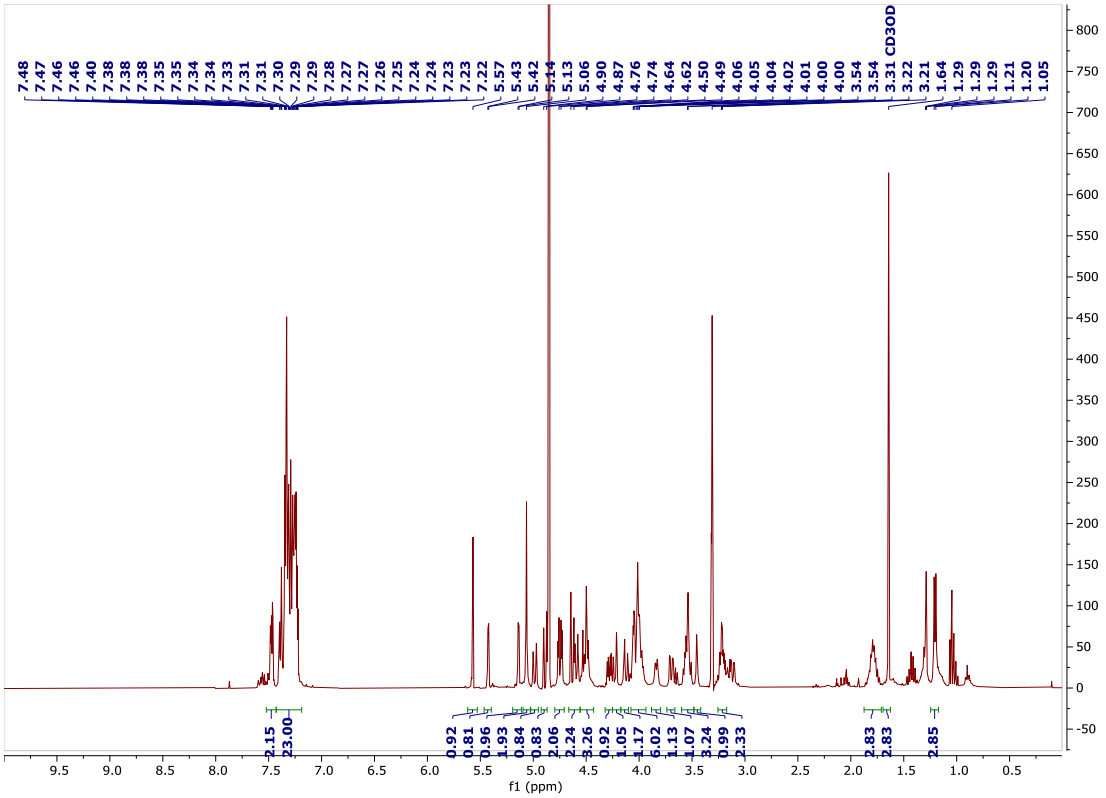

^{13}C-NMR (100 MHz, CD_3OD)

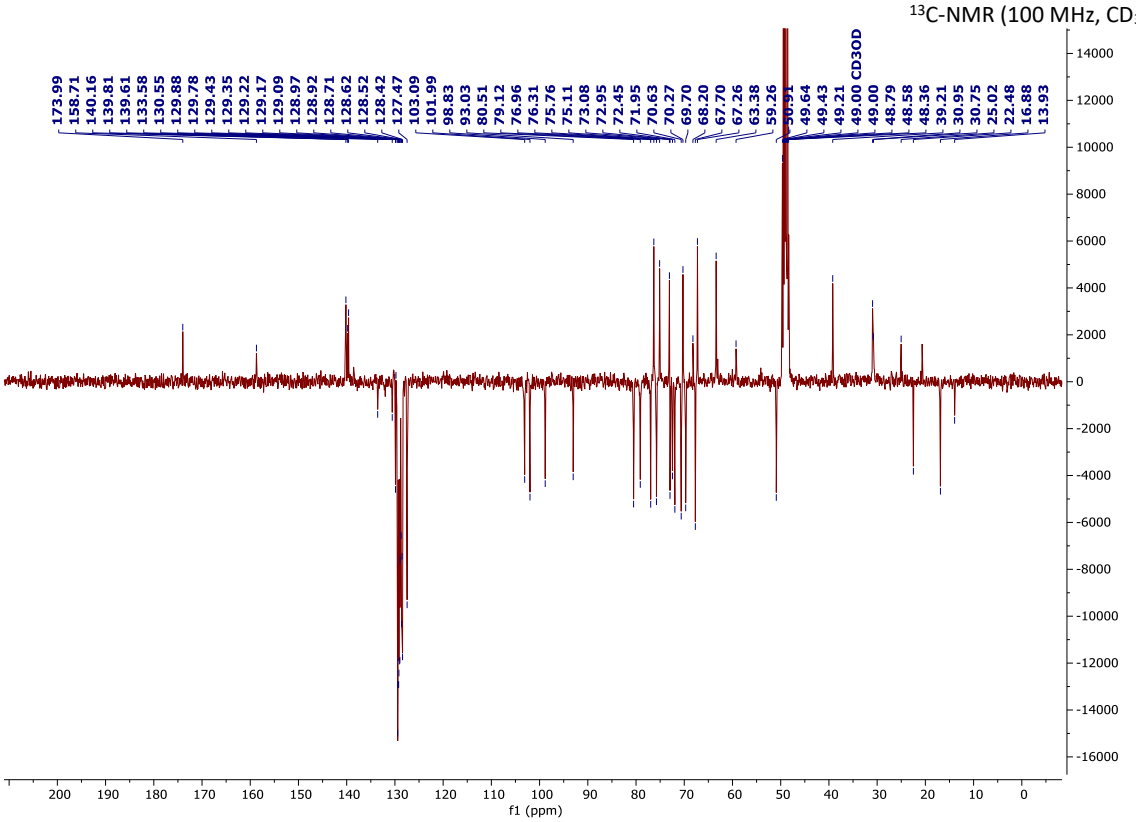

Compound 20

^{1}H-NMR (400 MHz, CD_3OD)

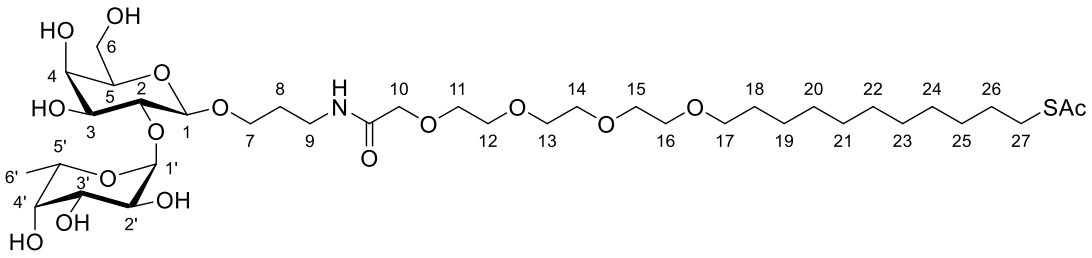

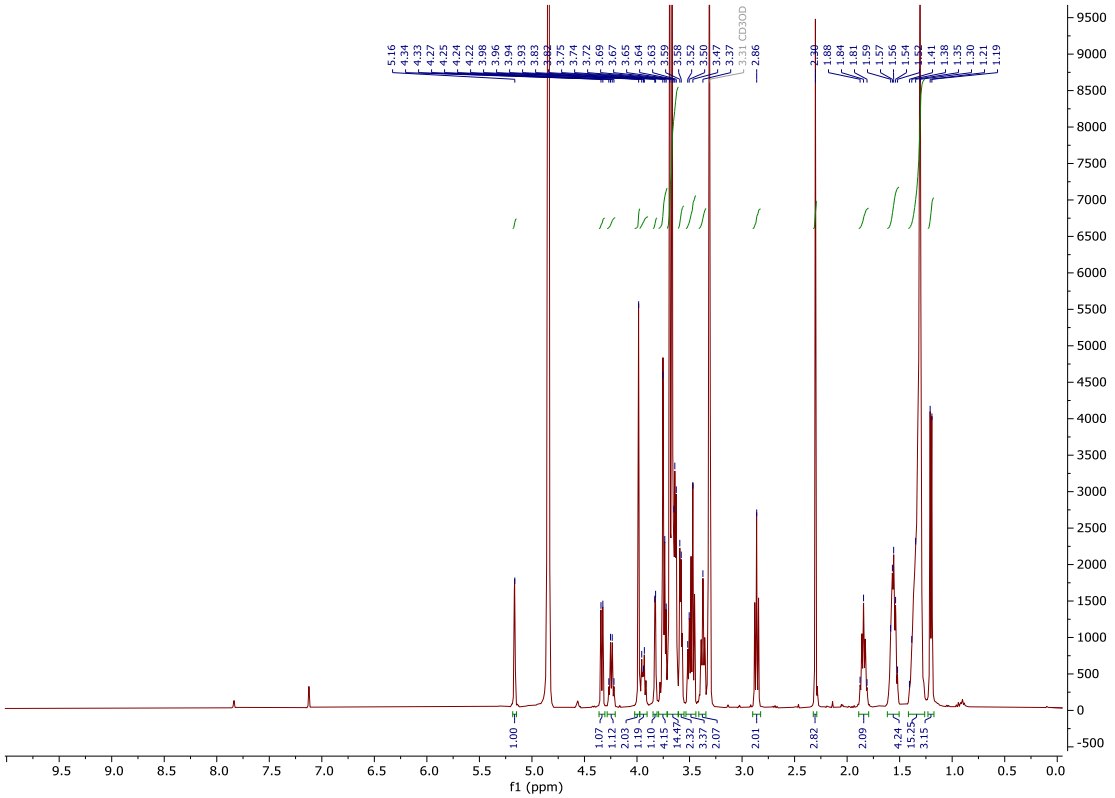

^{13}C-NMR (100 MHz, CD_3OD)

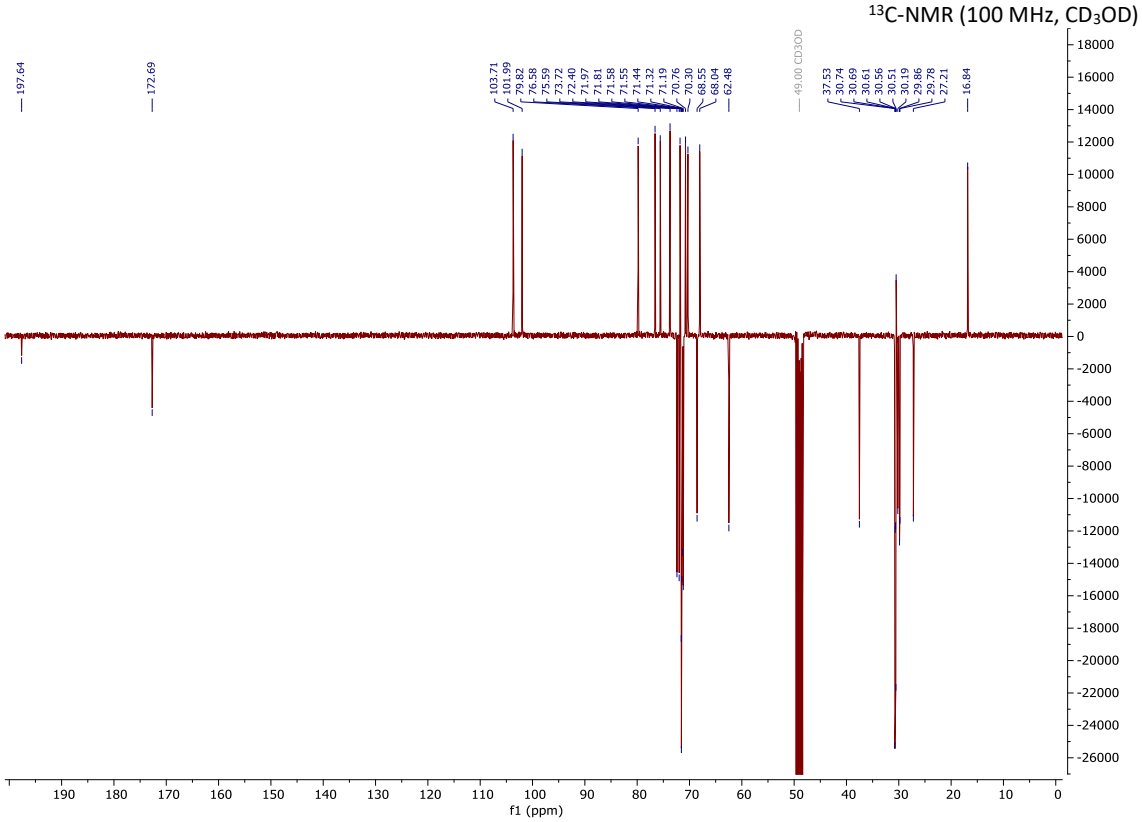

Compound 21

^{1}H-NMR (400 MHz, CD_3OD)

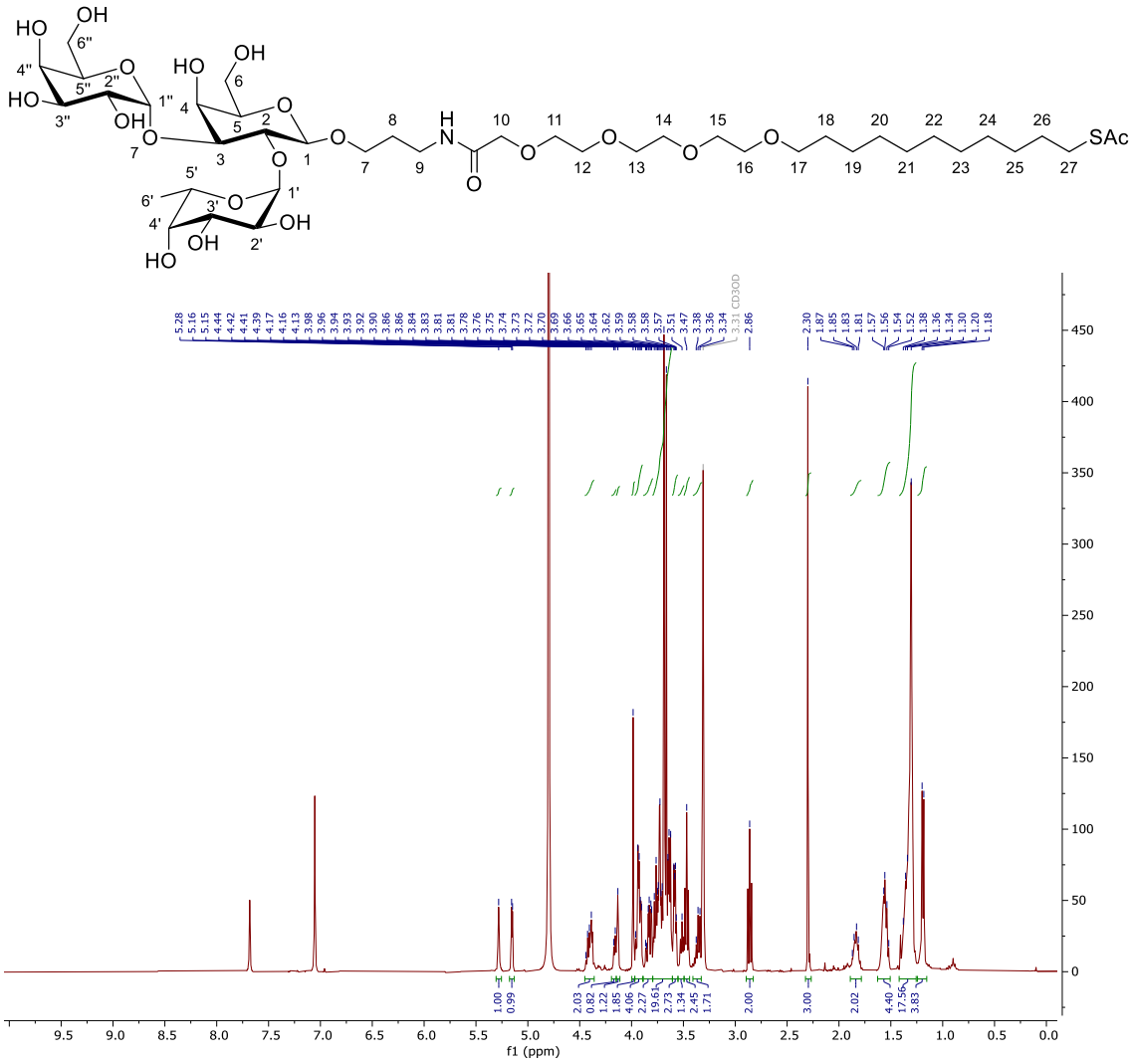

^{13}C-NMR (100 MHz, CD_3OD)

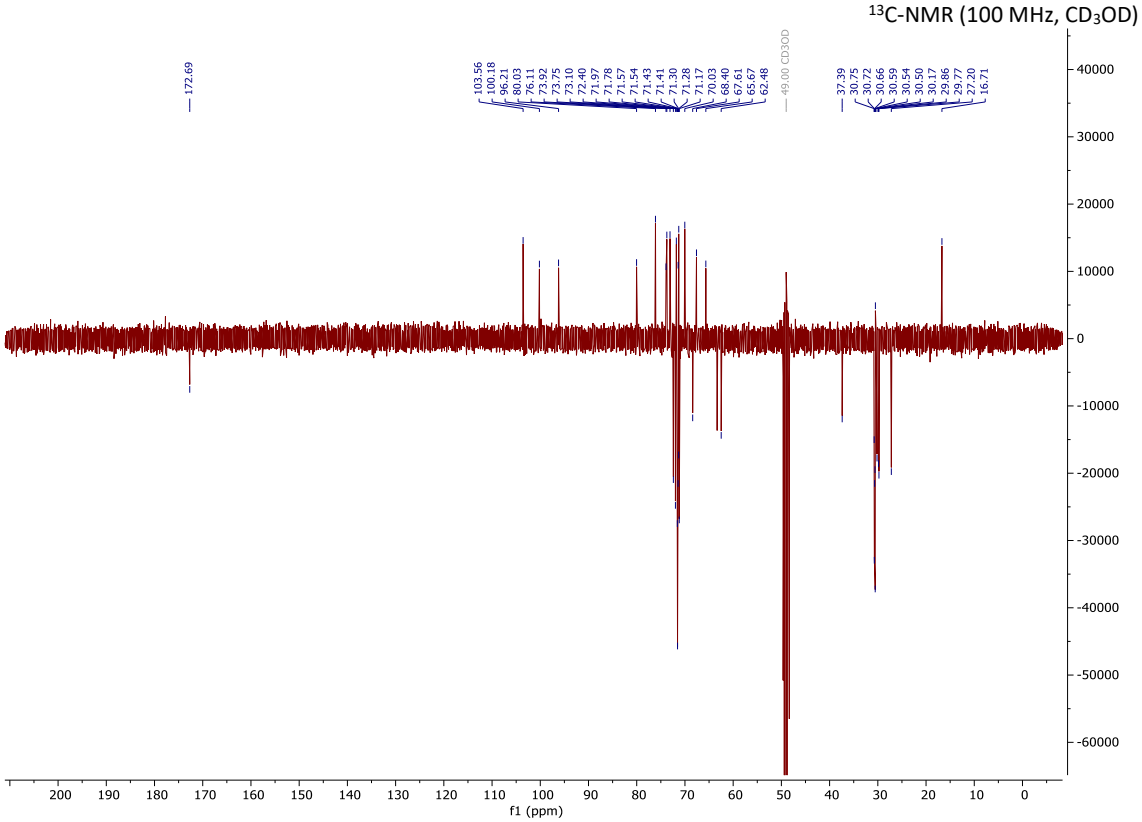

Compound 22

^{1}H-NMR (400 MHz, CD_3OD)

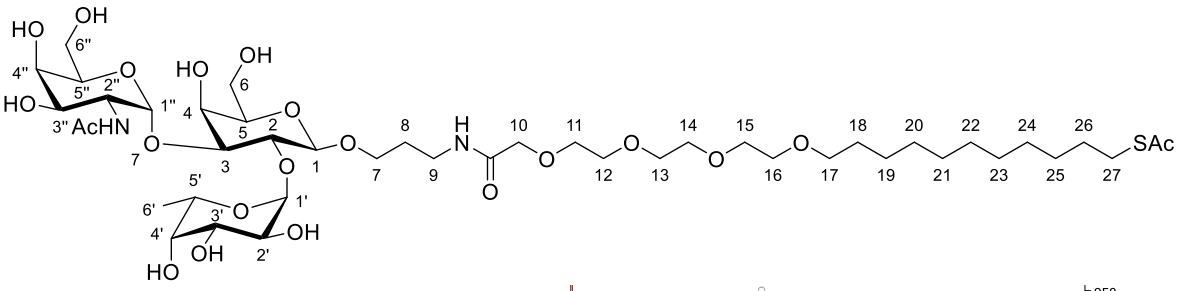

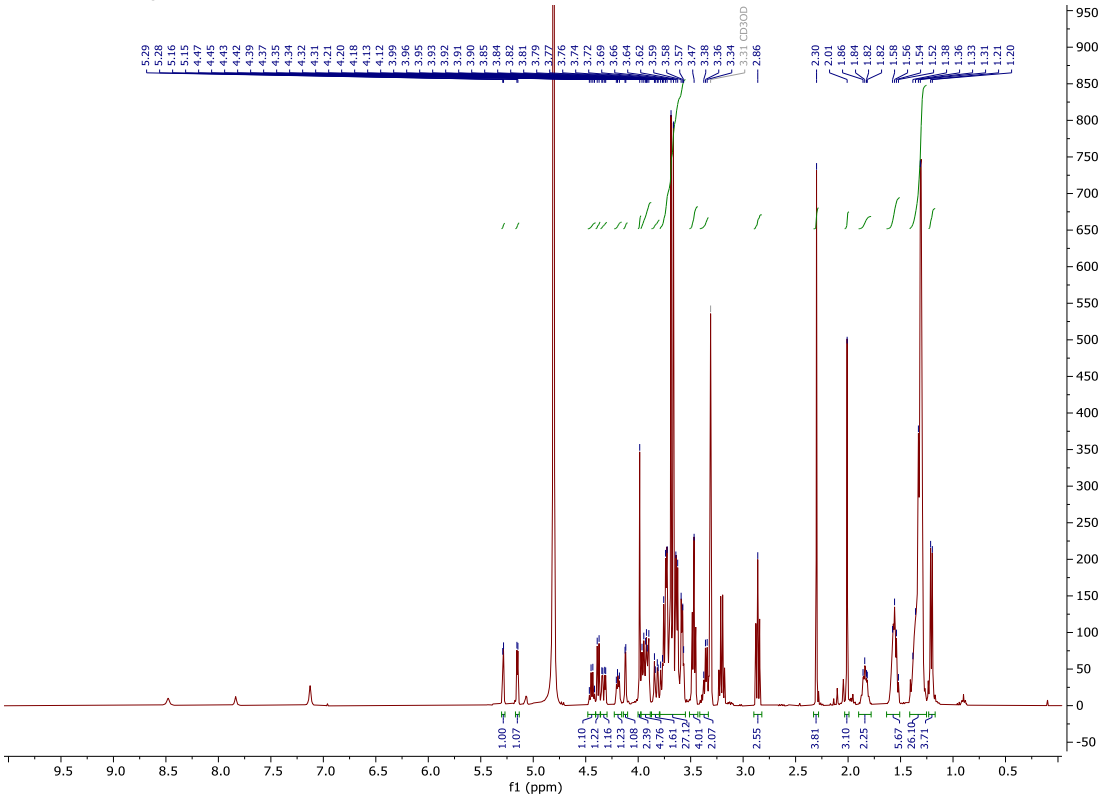

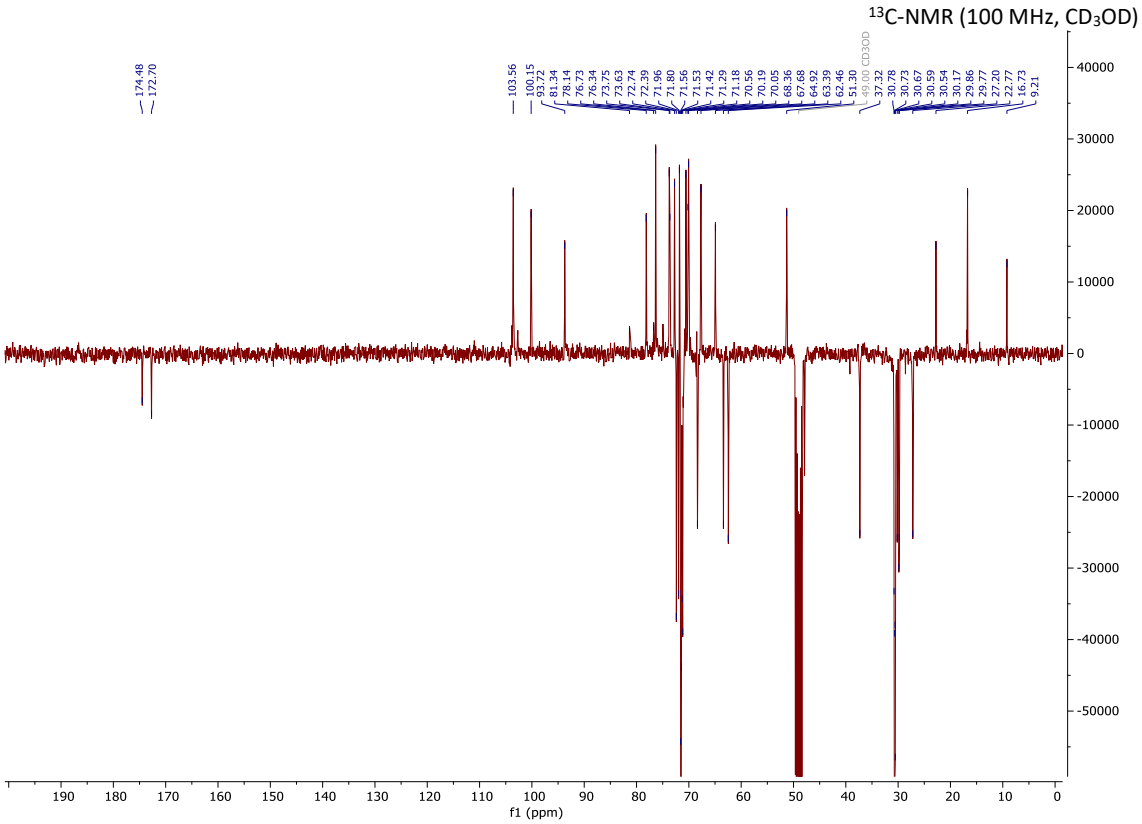

5. References

[1] G. Wider, L. Dreier, Measuring Protein Concentrations by NMR Spectroscopy, J Am Chem Soc 128 (2006) 2571–2576. https://doi.org/10.1021/ja055336t.

[2] E.O. Stejskal, J.E. Tanner, Spin Diffusion Measurements: Spin Echoes in the Presence of a Time-Dependent Field Gradient, J Chem Phys 42 (1965) 288–292. https://doi.org/10.1063/1.1695690.

[3] D. Li, G. Kagan, R. Hopson, P.G. Williard, Formula Weight Prediction by Internal Reference Diffusion-Ordered NMR Spectroscopy (DOSY), J Am Chem Soc 131 (2009) 5627–5634. https://doi.org/10.1021/ja810154u.

[4] T.A.A. Broadbent, Investigations on the theory of the Brownian movement. By A. Einstein. Pp. 122. $1.25. 1956 - The principles of mechanics. By H. Hertz. Pp. xlii, 274. $1.75. 1956 - Hydrodynamics. By H. L. Dryden, F. P. Murnaghan and H. Bateman. Pp. 634. $2.50. 1956. (Dover Publications, New York), The Mathematical Gazette 41 (1957) 231–231. https://doi.org/10.2307/3609228.

[5] K.E. Starling, The properties of gases and liquids, Third Edition, Robert C. Reid, John M. Prausnitz and Thomas K. Sherwood, McGraw-Hill (1977), 688 pages, $27.50, AIChE Journal 24 (1978) 1142–1142. https://doi.org/10.1002/aic.690240634.

[6] D.K. Wilkins, S.B. Grimshaw, V. Receveur, C.M. Dobson, J.A. Jones, L.J. Smith, Hydrodynamic Radii of Native and Denatured Proteins Measured by Pulse Field Gradient NMR Techniques, Biochemistry 38 (1999) 16424–16431. https://doi.org/10.1021/bi991765q.

[7] L. Ragona, O. Gasymov, A.J. Guliyeva, R.B. Aslanov, S. Zanzoni, C. Botta, H. Molinari, Rhodamine binds to silk fibroin and inhibits its self-aggregation, Biochimica et Biophysica Acta (BBA) - Proteins and Proteomics 1866 (2018) 661–667. https://doi.org/10.1016/j.bbapap.2018.03.009.